Distinct Intensification Pathways for a Shallow-Water Vortex Subjected to Asymmetric "Diabatic" Forcing

David A. Schecter[1*]

[1] *NorthWest Research Associates, Boulder, Colorado, USA*

Submitted January 4, 2020; Accepted in Revised Form June 1, 2020

Link to published journal article: https://doi.org/10.1016/j.dynatmoce.2020.101156

*Corresponding author address: NorthWest Research Associates, 3380 Mitchell Lane, Boulder, CO, USA, 80301. E-mail: schecter@nwra.com

Abstract

Observational studies and cloud resolving numerical simulations have shown that developing tropical cyclones often have markedly asymmetric distributions of moist convection. The present study uses a shallow-water model on the f-plane to gain further insight into the variety of vortex intensification pathways that may exist under such conditions. The diabatic forcing associated with asymmetric convection is represented by a localized mass sink displaced from the initial center of rotation. The pathway of vortex intensification is found to depend on whether the velocity-convergence generated by the mass sink exceeds a critical value s_c, and thereby prevents the escape of fluid that flows into the mass sink. The critical value is approximately given by $s_c = 2V_l/\rho_s$, in which ρ_s is the radial size of the mass sink, and V_l is the magnitude of the local vector-difference between the broader cyclonic velocity field and the drift velocity of the mass sink. If the convergence is supercritical so as to exceed s_c, the core of the vortex reforms in the vicinity of the mass sink and rapidly intensifies. Two other modes of intensification are found in subcritical systems. One common mode occurs at a moderate pace and entails a gradual drift of the vortex center toward the mass sink, coinciding with significant contraction of the radius of maximum azimuthal velocity. A slower mode can occur when a subcritical mass sink has substantial azimuthal drift. The slower mode resembles that expected for a symmetric system in which the mass sink is uniformly spread over its orbital annulus, whose radius from the vortex center is roughly constant over time. If the mass sink pulsates so as to periodically generate modestly supercritical values of convergence, a transition may occur from a subcritical mode of intensification to a supercritical mode as the pulsation period increases beyond a certain threshold. In a distinct set of simulations where the mass sink drifts radially outward from the initial vortex center with velocity $\dot{r}_s$, supercritical convergence determined with $V_l = \dot{r}_s$ in the formula for s_c is generally necessary for major vortex intensification.

Keywords: shallow-water model, nonlinear dynamics, vortices, tropical cyclone intensification

1. Introduction

Developing tropical cyclones misaligned by the continual or past action of environmental wind shear commonly have deep convection concentrated downtilt and well away from the center of the lower tropospheric circulation [e.g., Nguyen et al. 2017; Tao and Zhang 2014; Rappin and Nolan 2012; Molinari and Vollaro 2010]. The extent to which the outward displacement and asymmetric distribution of convection may hinder intensification of the cyclonic winds has not been fully elucidated. A complete theory should be able to predict the likelihood of transformative events that could jump-start intensification, such as vortex-core reformation where the localized deep convection resides [e.g., Chen et al. 2018; Nguyen and Molinari 2015]. The motivation for this paper is to gain further insight into various pathways of intensification and their conditions of applicability in vortices subjected to asymmetric diabatic forcing. To strengthen the conceptual foundation that may guide future investigations with cloud resolving simulations, we here revisit the fundamentals in the context of a shallow-water model on the f-plane.

Shallow-water and nondivergent barotropic models are often used to gain basic insight into various processes that are seen during the development of a tropical cyclone. Enagonio and Montgomery [2001] used a shallow-water model to shed light on how axisymmetrization processes affect intensification following the production of localized vorticity anomalies by convective bursts. Rozoff et al. [2009] used a nondivergent barotropic model to examine inner-core instabilities and the impact of subsequent vorticity mixing on the intensification of a vortex that is forced by an annular vorticity source representing the influence of convection in the azimuthal mean. Hendricks et al. [2014] conducted a similar study using a shallow-water model in which an annular mass sink replaced direct vorticity forcing; the mass sink locally amplified cyclonic vorticity by generating colocated convergence. Schubert et al. [2016] developed an analytical theory for the intensification of an axisymmetric shallow-water vortex forced by a mass sink that continually adjusts to the radial distribution of

potential vorticity. Lahaye and Zeitlin [2016] added a moisture equation to regulate the mass sink in a shallow-water model as they sought to improve upon earlier efforts to understand the nature and consequences of tropical cyclone instabilities [cf. Schecter 2018 and references therein]. The present study expands upon the foregoing line of research with a distinct emphasis on understanding the dynamics of shallow-water vortex intensification forced by a localized mass sink displaced from the initial center of rotation.

Of particular interest are the early and intermediate stages of tropical cyclone development. During this time period, the coupled asymmetric distributions of deep convection and horizontal velocity convergence in the lower part of the vortex can be strongly influenced by factors such as vertical misalignment that are not determined solely by low-level fluid variables. Because of this, it is deemed reasonable to let the mass sink representing convection be an independent element of the shallow-water model used herein to gain insight into the low-level dynamics of an immature, misaligned tropical cyclone. The independent mass sinks in our shallow-water vortices will generate convergence zones that vary in location, spatial extent and magnitude. They will either be static, pulsate, drift azimuthally or drift radially.

The primary objective will be to understand how variation of the convergence zone generated by an off-center mass sink affects the mechanism and time scale of vortex intensification. It will be shown that the prevailing mechanism is largely determined by whether the magnitude of convergence exceeds a critical value dependent on the size and drift velocity of the convergence zone, and on the local velocity of the broader cyclonic circulation. When having supercritical intensity, a convergence zone displaced from the central region of the cyclone will generally be found to induce on-site reformation of the vortex core and rapid intensification.[1] Systems possessing subcritical convergence zones will be found to follow one of two slower pathways of development. If the subcritical convergence zone has radial drift, the vortex may fail to experience more than a transient period of weak-to-moderate spinup. The preceding results are mostly new (to the author's knowledge) and will be thoroughly

[1]This paper does not restrict the term "rapid intensification" to a precise meteorological definition. The term merely refers to a process that is considerably faster than others to which it is compared.

explained in due course.

Despite focusing on a single-layer system, the dynamics to be studied may indirectly offer insights into the alignment of lower and upper circulations that often coincides with an acceleration of tropical cyclone intensification. Previous work has shown that adiabatic alignment can occur through the decay of three-dimensional vortex Rossby waves, just as the axisymmetrization of a shallow-water vortex can occur by the decay of two-dimensional vortex Rossby waves [e.g., Schecter and Montgomery 2003; Reasor and Montgomery 2015]. It is proposed here that additional analogies may exist between the various responses of a shallow-water vortex to an off-center mass sink and distinctly diabatic pathways of alignment found in cloud resolving tropical cyclone simulations [e.g., Nguyen and Molinari 2015; Chen et al. 2018; Rios-Berrios et al. 2018; Schecter and Menelaou 2020 (SM20)]. One of these diabatic alignment mechanisms involves reformation of the vortex core in an area of deep convection downtilt of the original surface-center of rotation. The conditions required for such an event to occur might include an analog of the supercritical convergence needed for the core reformation process that precedes rapid intensification in our shallow-water systems. Understanding the conditions for each of the two slower modes of intensification to occur in our subcritical shallow-water systems may also have relevance to the alignment problem. This is because the two modes are distinguished by whether the center of the shallow-water vortex (imagined to represent the lower part of a tropical cyclone) gradually approaches the mass sink (imagined to represent downtilt convection) or stays far away.

The remainder of this paper is organized as follows. Section 2 describes the forced shallow-water system and the numerics used to simulate its evolution. Section 3 explains the essential difference between flows produced by supercritical and subcritical mass sinks. Section 4 illustrates how this difference largely controls the pathway of vortex intensification in a variety of shallow-water systems. Section 5 elaborates on one of the slower subcritical modes of intensification with relatively subtle dynamics. Section 6 returns to the discussion started above regarding the potential relevance of the shallow-water dynamics to tropical

cyclone development. Section 7 summarizes the conclusions of this study. Appendix A briefly discusses a cloud resolving simulation that helped guide the construction of our simplified representation of deep convection (the mass sink) in section 2.2. Appendix B provides supplemental details of the computational setup. Appendix C reviews the behavior of symmetrically forced shallow-water vortices for comparison to the behavior of the asymmetric systems of present interest.

2. The Forced Shallow-Water Model

2.1 Fundamental Equations

The momentum and mass continuity equations in a shallow-water system are respectively given by[2]

$$\frac{\partial \mathbf{u}_*}{\partial t_*} + \boldsymbol{\eta}_* \times \mathbf{u}_* + \nabla_* \left(\frac{\mathbf{u}_*^2}{2} + g h_* \right) = \mathbf{F}_* \qquad \text{and} \tag{1a}$$

$$\frac{\partial h_*}{\partial t_*} + \nabla_* \cdot (\mathbf{u}_* h_*) = S_*, \tag{1b}$$

in which $\mathbf{u}_*(\mathbf{x}_*, t_*)$ is the horizontal velocity field, $h_*(\mathbf{x}_*, t_*)$ is the height of the free surface of the shallow-water layer, and $\boldsymbol{\eta}_*(\mathbf{x}_*, t_*) \equiv \nabla_* \times \mathbf{u}_* + f\hat{\mathbf{z}}$ is the absolute vorticity. As usual, ∇_* represents the horizontal gradient operator, $\hat{\mathbf{z}}$ is the vertical unit vector, $\mathbf{x}_*$ is the horizontal position vector, and t_* is time. The parameters f and g respectively denote the Coriolis parameter and the effective gravitational acceleration. The "diabatic forcing" S_* on the right-hand side of the continuity equation ideally accounts for the effects of moist convection and radiation. The area integral of the principal negative part of S_* (the mass sink) within a simulated vortex will be offset by that of a much weaker positive part spread over the entire domain so as to conserve total mass within the shallow-water system. A specific formula for S_* is forthcoming. The frictional effects of small scale turbulence and convective momentum

[2]The subscript $*$ is used here to distinguish dimensional variables and derivatives with respect to dimensional variables from their nondimensional counterparts appearing throughout the paper.

transport that could be incorporated into $\mathbf{F}_*$ will be neglected for this study.

It is convenient to reformulate the model and express all results in nondimensional variables. Let U (L) be the characteristic magnitude (length scale) of $\mathbf{u}_*$, LU^{-1} be the characteristic dynamical time scale, and H be the characteristic value of h_*. Substituting $\mathbf{u}_* \equiv U\mathbf{u}$, $h_* \equiv Hh$, $\mathbf{x}_* \equiv L\mathbf{x}$ ($\nabla_* \equiv L^{-1}\nabla$) and $t_* \equiv LU^{-1}t$ into Eq. (1a) with $\mathbf{F}_* = 0$ yields the following nondimensional momentum equation:

$$\frac{\partial \mathbf{u}}{\partial t} + \left(\nabla \times \mathbf{u} + \mathrm{Ro}^{-1}\hat{\mathbf{z}}\right) \times \mathbf{u} + \nabla \frac{\mathbf{u}^2}{2} + \mathrm{Fr}^{-2}\nabla h = 0, \tag{2a}$$

in which $\mathrm{Ro} \equiv U/Lf$ is the Rossby number and $\mathrm{Fr}^2 \equiv U^2/gH$ is the squared Froude number. By a similar procedure, we may write the nondimensional continuity equation as follows:

$$\frac{\partial h}{\partial t} + h\nabla \cdot \mathbf{u} + \mathbf{u} \cdot \nabla h = \frac{S_* L}{UH} \equiv S. \tag{2b}$$

We will focus on the parameter regime in which $\mathrm{Ro} \gtrsim 1$ and $\mathrm{Fr}^2 \ll 1$. All tropical cyclones satisfy the preceding condition on Ro. The small Froude number assumption may be more appropriate for immature systems than for strong hurricanes.

Equation (2a) suggests that the perturbation of the nondimensional height field from its value h_p at the periphery of a shallow-water vortex in the parameter regime of interest is of order Fr^2. Let us further assume that the temporal deviation of h_p from its initial value h_0 is no greater than order Fr^2. If in addition $S \gg \mathrm{Fr}^2$, Eq. (2b) would suggest that

$$\nabla \cdot \mathbf{u} \to S/h_0 \tag{3}$$

as the Froude number asymptotically approaches zero. In the same limit, the frictionless vorticity equation [the curl of Eq. (2a)] can be simplified as follows:

$$\begin{aligned} \frac{\partial \zeta}{\partial t} + \mathbf{u} \cdot \nabla \zeta &= -\eta \nabla \cdot \mathbf{u} \\ &\to -\eta S/h_0, \end{aligned} \tag{4}$$

in which $\zeta \equiv \hat{\mathbf{z}} \cdot (\nabla \times \mathbf{u})$ and $\eta \equiv \zeta + \mathrm{Ro}^{-1}$. The velocity $\mathbf{u}$ remaining in the advective term can

be diagnosed from knowledge of ζ and the imposed forcing S using the Helmholtz formula, $\mathbf{u} = \hat{\mathbf{z}} \times \nabla\psi + \nabla\chi + \mathbf{u}_a$. The streamfunction ($\psi$) and velocity potential (χ) appearing in this formula are solutions to $\nabla^2\psi = \zeta$ and $\nabla^2\chi = S/h_0$ with appropriate boundary conditions that also determine the irrotational nondivergent velocity correction $\mathbf{u}_a$ [see section 5.2]. It is evident that as $\mathrm{Fr}^2 \to 0$, Eq. (4) may serve as the sole prognostic equation for the vortex evolution. This simplified model has some computational advantages in filtering out gravity waves, but we will reserve its use primarily for theoretical considerations.

Although characteristic scales may change as a simulated vortex intensifies under the influence of a mass sink, a fixed nondimensionalization will be used hereafter. Specifically, U and L will equal the initial maximum azimuthal velocity of the vortex and the initial radius at which the maximum velocity occurs. H will equal the initial height of the shallow-water layer beyond the outer boundary of the vortex, where the velocity field is zero. Note that the preceding choice for H implies that $h_0 = 1$. Choosing U and L to match the characteristics of the vortex at the end of any simulation conducted for this study would increase the Froude and Rossby numbers, but the former would remain small compared to unity.

2.2 Formulation of the Mass Sink

There are many possible formulations of the forcing S that appears in the continuity equation. The formulation used here may well have broader relevance, but is conceived for studies that aim to provide insight into the early development of the lower tropospheric circulation of a misaligned tropical cyclone having deep convection concentrated in a localized region downtilt of the surface vortex center [e.g., appendix A]. Although the lower tropospheric irrotational wind associated with deep convection has both convergent and divergent parts, we here assume that the convergent part dominates in the vortex core.

The basic form of the forcing used in this study to create off-center convergence similar

to that associated with downtilt convection is expressed as follows:

$$S/h_0 = -s\Theta\left(\rho_s - |\mathbf{x} - \mathbf{x}_s|\right) + s\pi\rho_s^2/A_d, \tag{5}$$

in which $\Theta(\kappa) = 1$ (0) for positive (negative) κ, $A_d \gg \rho_s^2$ is the area of the simulation domain, and all other variables are defined below. The first term on the right-hand side of Eq. (5) is a uniform circular mass sink of radius ρ_s centered at a position $\mathbf{x}_s$ within the vortex core. The second term is added to restore lost mass to the shallow-water layer uniformly over the simulation domain; it is not uncommon to relate such a mass source to radiative cooling [e.g., Ooyama 1969]. We will restrict our attention to mass sinks with magnitudes given by

$$s = s_o + s_p \sin^2\left(\pi t/\tau_p\right). \tag{6}$$

The first term (s_o) is constant in time. The second term is a squared sinusoidal pulsation whose amplitude and wave period are s_p and τ_p, respectively. Note that both s_o and s_p are assumed to be non-negative. The mass sink will be allowed to revolve around the initial vortex center (the domain center) $\mathbf{x}_{c0}$ and move radially outward. The specific formula for the position vector of the sink center will be given by

$$\mathbf{x}_s(t) - \mathbf{x}_{c0} = r_s(t)\left[\cos(\Omega_s t)\hat{\mathbf{x}} + \sin(\Omega_s t)\hat{\mathbf{y}}\right], \tag{7}$$

in which $\hat{\mathbf{x}}$ and $\hat{\mathbf{y}}$ are orthonormal Cartesian basis vectors, r_s is a time-dependent domain-centered orbital radius, and Ω_s is a constant angular frequency. We will assume that $r_s = r_{s0} + \dot{r}_s t$, in which r_{s0} and $\dot{r}_s$ are constants. It is worth remarking that a sizeable number of simulations will let r_{s0} equal the initial radius at which the azimuthal velocity of the vortex is peaked. This particular setting is motivated by the proximity of deep convection and maximal winds found in a recent study of misaligned tropical cyclones [SM20]; the reader may consult appendix A for an illustrative example. Bear in mind that even if $\dot{r}_s = 0$, the distance between the mass sink and the mobile center of rotation will usually change over time and thereby differ from r_{s0} [see section 4.2.3].

One might have considered using an alternative model that self-regulates the diabatic forcing associated with convection, which is presently imposed through S. Such an approach commonly involves a parameterization of convection dependent on supplemental equations for moist-thermodynamic fluid variables that duly incorporate oceanic surface fluxes [e.g., Ooyama 1969; Zehnder 2001; Schecter 2011; Lahaye and Zeitlin 2016; Rostami and Zeitlin 2018]. Self-regulation of the diabatic forcing would also require moving beyond a one-layer system, if vertical misalignment of the vortex has a role in organizing the asymmetric convection of interest.[3] But achieving the objectives of this study does not require a model more advanced than that presented above. To answer how the properties of a convergence zone affect intensification, we may simply vary those properties directly and examine the responses of the vortex. In the small Froude number regime where Eq. (3) is valid, specifying the properties of the convergence zone is tantamount to specifying the properties of the mass sink. We will consider a sufficiently broad range of mass sink parameters to uncover a variety of vortex intensification pathways with potential relevance to asymmetric tropical cyclone development.

Note finally that the mass sink in our model has no safety switch. Its continual operation can intensify a vortex beyond natural limits and lead to locally zero fluid depth. For all cases considered herein, such breakdown of the model occurs after the dynamics of interest.

2.3 The Initial Vortex

Description of the initial conditions and vortex dynamics requires the introduction of a polar coordinate system in which r and φ respectively denote the radial and azimuthal coordinates, while u and v respectively denote the radial and azimuthal velocity fields. The initial state of all systems considered herein consists of an azimuthally symmetric cyclone

[3]This is not to say that one-layer models are incapable of generating localized off-center convection through mechanisms unrelated to vertical misalignment. For example, the one-layer model of Lahaye and Zeitlin [2016] produced localized off-center convection in the aftermath of a circular shear-flow instability.

whose vorticity distribution is of the form

$$\zeta = \zeta_o \left[e^{-\gamma r^2} - \frac{1 - e^{-\gamma r_b^2}}{\gamma r_b^2} \right] \Theta(r_b - r), \tag{8}$$

in which $\zeta_o = 3.575$, $\gamma = 1.179$ and $r_b = 5.525$. The corresponding azimuthal velocity is given by

$$v = \frac{1}{r} \int_0^r d\tilde{r} \tilde{r} \zeta(\tilde{r}) = \frac{\zeta_o}{2\gamma r} \left[1 - e^{-\gamma r^2} - \frac{1 - e^{-\gamma r_b^2}}{r_b^2} r^2 \right] \Theta(r_b - r). \tag{9}$$

The aforementioned combination of values for ζ_o, γ and r_b ensures that the maximum of v is 1 at $r = 1$. The initial radial velocity u is set to zero. The initial distribution for h is determined by the requirement of gradient balance,

$$\frac{dh}{dr} = \mathrm{Fr}^2 \left(\frac{v^2}{r} + \frac{v}{\mathrm{Ro}} \right), \tag{10}$$

in conjunction with the condition $h = 1$ for $r \geq r_b$. Figure 1 depicts the initial structure of the cyclone for Ro=1.47 and arbitrary Fr.[4]

2.4 Numerics

Numerical integrations of the shallow-water equations are as in Schecter and Montgomery [2006] with the straightforward addition of S in the continuity equation. The integration technique is based on the enstrophy-conserving staggered grid model of Sadourny [1975]. The flow is evolved forward in time using a fourth-order Runge-Kutta method. Hyperdiffusion is employed to dissipate grid-scale fluctuations and ensure numerical stability. At radii well beyond r_b, a sponge-ring partially absorbs outward propagating inertia-gravity waves and keeps the peripheral fluid near rest.

The simulation domain is a square box with doubly periodic boundary conditions. The

[4]Needless to say, Fr must be sufficiently small to prevent the solution of Eq. (10) for h from becoming negative as r tends toward zero.

fluid variables are distributed on two nested square grids. The inner and outer grid lengths are approximately 6 and 20 times the cyclone's initial radius of maximum azimuthal velocity. In the same units, the inner grid spacing δx is approximately 0.01. The outer grid spacing of $6\delta x$ is relatively large but adequate for resolving the outer flow in our simulations. Appendix B provides a more precise and complete specification of the computational parameters.

2.5 Vortex-Centered and Sink-Centered Reference Frames

The structure of a shallow-water cyclone is often analyzed in a moving vortex-centered reference frame. The vortex center $[\mathbf{x}_c(t)]$ serving as the origin of the coordinate system is found here by a variant of a commonly used algorithm. The streamfunction ψ of the rotational flow is computed from the vorticity distribution on a uniform mesh with grid spacing δx covering the entire doubly periodic domain, and is defined to have a mean value of zero. The search region is limited to where ψ is negative and less than a specific fraction (usually eight-tenths) of its instantaneous minimum value. The location of $\mathbf{x}_c$ is provisionally equated to the grid point in the search region where centering a polar coordinate system maximizes the peak value of $\bar{v}(r)$, defined as the φ-averaged azimuthal velocity distribution. If shifting the coordinate center a distance $\delta x/2$ in any grid direction increases the peak value of $\bar{v}$, $\mathbf{x}_c$ is reset to this more appropriate location. Searching for the peak value of $\bar{v}$ is generally restricted to $r \geq r_c$, in which r_c is a minimum core radius to be specified and discussed in section 4.2.

A sink-centered reference frame is sometimes more convenient for theoretical discussions. As the name implies, the coordinate center of this reference frame coincides with the center of the moving mass sink. The velocity of the sink-centered reference frame relative to a stationary observer is thus given by $\dot{\mathbf{x}}_s \equiv d\mathbf{x}_s/dt$.

3. Basic Theory of Supercritical and Subcritical Mass Sinks

The properties of convection and lower tropospheric convergence within a developing tropical cyclone may vary considerably from case to case, owing to different histories of the storm systems and different environmental conditions such as sea-surface temperature and vertical wind shear. With the variability of diabatic forcing there may exist more than one pathway of vortex intensification. It is found that the specific pathway of intensification in our shallow-water model crucially depends on the initial flow structure in the vicinity of the mass sink. The present section describes two basic flow structures of central importance, their conditions of applicability, and their theoretical consequences. Some simplifications are made to reduce the mathematics and to facilitate the introduction of key concepts. The discussion starts by considering highly localized, non-pulsating mass sinks that are positioned well away from the center of the vortex. Other scenarios are addressed later on.

3.1 Off-Center Sinks

To begin with, assume that the Froude number is sufficiently small for the applicability of Eqs. (3) and (4). Furthermore, let $s_p = 0$ in order for the magnitude of the mass sink to maintain a constant value (s_o) over time. Let us also suppose that $\rho_s \ll r_s \sim 1$. Then, to a reasonable approximation, one may eliminate spatial variation from the velocity field of the broader cyclone in the local region of the mass sink.

Let $\mathbf{u}_l \equiv \mathbf{u} - \dot{\mathbf{x}}_s$ denote the local fluid velocity field in the sink-centered reference frame. In addition, let (ρ, θ) denote a polar coordinate system centered at $\mathbf{x}_s$, with $\theta = \pi/2$ corresponding to the initial direction of $\mathbf{u}_l$ at $\rho = 0$.[5] With the preceding conventions, the initial

[5]Initially, if the mass sink is not exceptionally strong, $\mathbf{u}_l$ at its center is virtually equivalent to $\mathbf{u}_l$ at large radii. Note that a "large" radius ρ in a local context satisfies $\rho_s \ll \rho \ll r_s$.

local velocity field can be written as follows:

$$\mathbf{u}_l = \left(V_l \sin\theta - \frac{s_o \rho_s}{2} \frac{\rho_<}{\rho_>} \right) \hat{\boldsymbol{\rho}} + V_l \cos\theta \hat{\boldsymbol{\theta}}, \tag{11}$$

in which $V_l \equiv |\mathbf{u}_l(\rho = 0)| = \{[\bar{v}(r_s) - r_s\Omega_s]^2 + \dot{r}_s^2\}^{1/2}$, and $\rho_>$ ($\rho_<$) is the greater (lesser) of ρ and ρ_s. For the systems considered herein, $\bar{v}$ in the preceding formula for V_l corresponds to the right-hand side of Eq. (9). It should be mentioned that Eq. (11) tacitly neglects a small correction to the divergent component of $\mathbf{u}_l$ associated with the second term on the right-hand side of Eq. (5), under the implicit assumption that $\rho \ll \sqrt{A_d}$.

Stagnation points of $\mathbf{u}_l$ exist where both of its components are zero. Vanishing of the azimuthal component requires that $\theta = (2n-1)\pi/2$, in which $n \in \{1, 2\}$. Vanishing of the radial component requires that $n = 1$ and

$$s_o = \frac{2V_l}{\rho_s} \frac{\rho_>}{\rho_<}. \tag{12}$$

The preceding equation can be solved only if s_o is greater than or equal to the critical value

$$s_c \equiv \frac{2V_l}{\rho_s}, \tag{13}$$

in which case the stagnation radii occur at $\rho = \rho_\pm \equiv \rho_s(s_o/s_c)^{\pm 1}$. The outer stagnation point at ρ_+ is a saddle point, whereas the inner stagnation point at ρ_- is a *point of attraction* in the sense that it pulls in nearby fluid from all directions. Henceforth, a mass sink initially possessing (lacking) a point of attraction will be called *supercritical* (*subcritical*). Similar terminology will be used to describe the resulting dynamics.

Figure 2a shows the initial streamlines of $\mathbf{u}_l$ in the neighborhood of a selected supercritical mass sink. In the imaginary scenario of a frozen velocity field, the region of fluid flowing to the point of attraction is bounded by a separatrix emanating from the outer stagnation point. An equation for the separatrix is readily obtained from the streamfunction ψ of the outer nondivergent velocity field. The streamfunction outside the mass sink is

defined implicitly by $\mathbf{u}_l \equiv \hat{\mathbf{z}} \times \nabla\psi$, and given explicitly by

$$\psi(\rho, \theta) = \frac{s_o \rho_s^2}{2}\theta + V_l \rho \cos\theta, \tag{14}$$

in which $\rho > \rho_s$ and $-\pi/2 < \theta \leq 3\pi/2$. The equation for the separatrix is given by $\psi(\rho, \theta) = \pi s_o \rho_s^2/4$, in which the right-hand side corresponds to that of Eq. (14) evaluated at the outer stagnation point $(\rho_+, \pi/2)$. As $\rho \to \infty$, the separatrix equation can be solved only if $\theta \to -\pi/2$ or $3\pi/2$. Let $\tilde{x} \equiv \rho\cos\theta$, and define the half-width of the separatrix $\tilde{x}_+$ by the limit of $|\tilde{x}|$ as $\rho \to \infty$ along the separatrix. By Eq. (14) and our previous considerations, we obtain $\tilde{x}_+ = \pi\rho_s s_o/s_c = \pi\rho_+$. It is worth remarking that for a mass sink with a non-negative radial drift velocity $\dot{r}_s$, the outer stagnation point will be displaced from $\mathbf{x}_s$ toward the center or along the local tangent of the broader cyclonic flow. It follows that the local overlap between the region of fluid drawn into the mass sink and the inward section of the broader cyclone will have a characteristic length scale of ρ_+ or $\tilde{x}_+$. Either way, the length scale of the overlap is of order $\rho_s s_o/s_c$.

Assuming that it persists, the existence of a point of attraction within the mass sink when $s_o > s_c$ is expected to have major dynamical consequences. Without a point of attraction, Lagrangian fluid elements pass through the mass sink [see Fig. 2b] and transport their moderately amplified vorticity to other regions of the broader cyclone. With a point of attraction, fluid elements flowing into the mass sink get trapped. Equation (4) suggests that vorticity in the vicinity of the point of attraction will grow in a manner similar to $\zeta \sim \zeta_l e^{s_o t}$, in which ζ_l depends on local conditions at $t = 0$ and a constant additive correction has been ignored. With this in mind, it is reasonable to hypothesize that the rotational center of a cyclone containing a supercritical mass sink will jump to a relatively small but intense vorticity core that emerges in the neighborhood of the mass sink by a time proportional to s_o^{-1}. Following the formation of a new central core, the cyclone should continue to intensify on a similar time scale. By contrast, we anticipate slower and possibly incomplete motion of the rotational center toward a subcritical mass sink. Moreover, since fluid escapes

the vorticity amplification process in a subcritical mass sink, we anticipate a less efficient mode of vortex intensification.

The prediction that supercriticality ($s_o > s_c$) should enable local convergence to trap fluid in the mass sink and thereby activate fast vortex intensification by way of core reformation seems consistent with basic dynamical considerations. It is readily seen that $\tau_c \equiv s_c^{-1} = \rho_s/2V_l$ is the time required for the background flow in the sink-centered reference frame to advect a fluid parcel across one-half the radius of the mass sink. Furthermore, $\tau_o \equiv s_o^{-1}$ is one-half the exponential decay time for the radius of a circular ring of fluid within an isolated mass sink. Without having conducted a detailed analysis of the flow structure in the vicinity of the mass sink, one might have reasonably guessed that fluid trapping should occur when τ_o is appreciably less than τ_c, or equivalently when s_o appreciably exceeds s_c.

Note that there are several ways to transition from subcritical to supercritical dynamics. One way is to increase the magnitude (s_o) of the mass sink . Another way is to increase the core radius ρ_s of the mass sink. A third way is to reduce V_l by changing r_{s0}, Ω_s or $\dot{r}_s$.

3.2 Pulsating and Initially Centered Sinks

The condition for supercritical dynamics is generally more subtle for a pulsating mass sink. To simplify the discussion, suppose that the offset s_o of the squared sinusoidal pulsation is set to zero, so that the sink magnitude oscillates between 0 and s_p [see Eq. (6)]. The condition $s_p > s_c$ would seem to be required for a point of attraction to appear within the mass sink during part of the oscillation cycle, and is presumably necessary for supercritical dynamics. If the wave period τ_p is much less than τ_c, one might also expect to find that $s_p/2 > s_c$ is a sufficient condition for supercritical dynamics, considering that $s_p/2$ is the time average of s over each successive pulse. The seemingly more complicated scenario in which $s_p/2 < s_c < s_p$ and τ_p is arbitrary will be examined in section 4.2.4.

On another matter, it is natural to question whether the condition for supercritical dynamics derived for systems with non-pulsating mass sinks in section 3.1 remains valid

as $r_s \to 0$. In the preceding limit, any formal theory that includes a nonzero contribution of the broader cyclone to the local flow would have to take into account its curvature and radial variation. On the other hand, suppose that a mass sink initialized with $r_s = 0$ drifts outward with a radial velocity $\dot{r}_s$ of order unity. Since the magnitude of the velocity field of the broader cyclone near $r = 0$ is substantially less than unity, $-\dot{r}_s\hat{\mathbf{x}}$ would provide the main contribution to the local background flow observed in the sink-centered reference frame. Under this scenario, $\tau_c = \rho_s/(2\dot{r}_s)$ is a good approximation for the time scale of background advection across the mass sink. Moreover, $\tau_o = s_o^{-1}$ still provides a reasonable estimate for the characteristic time scale of inflow within the mass sink. Thus, the basic expectation of supercritical dynamics when $\tau_o < \tau_c$ remains consistent with the condition $s_o > s_c$, with $V_l = \dot{r}_s$ in the definition of s_c. The foregoing expectation will be tested for systems in which $\dot{r}_s$ is comparable to unity (as supposed) or moderately smaller. Note that a mass sink with $r_s = \dot{r}_s = 0$ is supercritical for any s_o owing to a point of attraction at $\rho = 0$.

4. Simulations of Cyclones with Supercritical and Subcritical Mass Sinks

4.1 The Data Set

A large number of numerical simulations have been conducted to verify the predicted transition from slow to fast modes of vortex intensification as the status of the mass sink changes from being subcritical to supercritical. Each simulation belongs to one of four groups that are distinguished by the time dependence and motion of the mass sink. The mass sink is either Stationary and Time-Independent (STI), Pulsating (P), Azimuthally Drifting (AD), or Radially Drifting (RD).

Table I summarizes the pertinent parameters of each simulation group. All simulations are initialized to have Froude numbers much less than unity and Rossby numbers of order unity. Furthermore, all mass sinks have small radii relative to the cyclone's initial radius of maximum velocity ($\rho_s \ll 1$). The STI, AD and RD mass sinks do not pulsate ($s_p = 0$) and

have static magnitudes (values of s_o) straddling the critical value s_c. The STI mass sinks are distinguished by having $\Omega_s = \dot{r}_s = 0$. The AD mass sinks have zero radial velocity ($\dot{r}_s$) relative to the initial vortex center, but have finite angular velocities (values of Ω_s) ranging from 0.25 to 0.75 times the initial characteristic cyclone rotation frequency. The RD mass sinks have zero angular velocity, and radial velocities between 0.25 and 1 times the initial maximum velocity of the cyclone. Moreover, the RD mass sinks differ from all others in having no initial displacement from the vortex center ($r_{s0} = 0$). The P mass sinks are stationary and off-center like the STI mass sinks, but are distinguished in having $s_o = 0$ and a finite pulsation amplitude. The selected pulsation amplitude ($s_p = 1.33 s_c$) yields peak and pulse-averaged intensities that are respectively above and below s_c. The scaled wave period ($s_c \tau_p$) varies over three orders of magnitude, from 0.2 to 150.

Figure 3 illustrates possible positions and drifts of various mass sinks within a simulated shallow-water system. The properties of the mass sinks including their magnitudes are intentionally diverse to cover a broad spectrum of scenarios that may be relevant to a developing tropical cyclone. Appendix A illustrates the potential relevance of a quasi-stationary mass sink and the associated off-center convergence zone over a prolonged period of vortex evolution. Drifting mass sinks are deemed analogous to drifting concentrations of cumulus activity that are commonly found in cloud resolving simulations of asymmetric tropical cyclone development amid environmental wind shear [e.g., Rios-Berrios et al. 2018; Tao and Zhang 2014; Rappin and Nolan 2012]. One notable result of the forthcoming computational survey will be an explicit demonstration of how substantial drift of the mass sink and the associated convergence zone can radically change the mode and effectiveness of subcritical intensification. Simulations in the supercritical parameter regime will not only verify the theoretical prediction of faster vortex spinup, but could also prove useful for understanding plausibly realistic intensification pathways that involve core reformation [see section 6]. Although the majority of simulations have mass sinks with time-independent magnitudes to facilitate discussion of the essentials of asymmetric intensification, pulsating mass sinks are included

in the computational survey to touch upon the less purified dynamics of natural systems where convection may wax and wane on a range of time scales.

4.2 Intensification Forced by Off-Center Mass Sinks

The present subsection considers the intensification of vortices containing off-center mass sinks with $\dot{r}_s = 0$ and hence $r_s = r_{s0}$. The time scale for intensification is equated to the time required for the maximum value of $\bar{v}$ beyond a minimum core radius r_c (in the vortex-centered coordinate system) to increase by a factor of 3, and is denoted t_3. In relation to tropical cyclone development, t_3 is comparable to the time required for a tropical depression to become a modest hurricane. The minimum radius $r_c = 0.138$ is imposed on the search for the maximum azimuthal velocity, because the supercritical intensification process typically leads to the formation of exceptionally small tornado-like vortices near the point of attraction. The present study is more concerned with intensification on length scales no smaller than the eyewall radius of a mature hurricane, which is unlikely to be smaller than one-tenth the length scale of the tropical depression.

4.2.1 Cyclones with Stationary Time-Independent Mass Sinks

Consider first the intensification of cyclones with STI mass sinks displaced from $\mathbf{x}_{c0}$ by a distance equal to the initial radius of maximum azimuthal velocity, such that $r_s = 1$. Figure 4 illustrates the variation of the scaled intensification time $s_o t_3$ with the ratio of s_o to the theoretical critical value s_c. The variation is shown separately for systems with $\rho_s = 0.18$ [Fig. 4a] and $\rho_s = 0.37$ [Fig. 4b]. Filled data points are for cyclones whose initial conditions yield Fr=0.042 and Ro=1.47; unfilled data points are for cyclones initialized with twice the strength in the same environment. The scaled intensification time invariably decays as s_o/s_c increases from 0.33 to unity, whereupon it remains nearly constant. The decay is roughly 3-fold (2-fold) for $\rho_s = 0.18$ (0.37), regardless of the initial vortex strength.

Figure 5 illustrates the sensitivity of the preceding results to the location of the mass sink. Here the data are confined to cyclones whose initial conditions yield Fr=0.042 and Ro=1.47, irrespective of whether the mass sink is relatively small [Fig. 5a] or large [Fig. 5b]. Increasing r_s to 2.17 generally extends the time required for intensification. Increasing r_s also moves the end point of the transition from slow to fast intensification to a value of s_o/s_c that measurably exceeds unity. The end point moves farther beyond unity when the mass sink is relatively small. Decreasing r_s to 0.38 drops $s_o t_3$ closer to a semi-analytical prediction for axisymmetric intensification in the limit $r_s \to 0$, shown by the dashed line and explained in appendix C2. Slower development is still discernible at subcritical values of s_o, but the slowdown is minimal for systems with the larger mass sink. The latter result is unsurprising given that the reduction of r_s causes the larger mass sink to nearly overlap the initial center of the cyclone.

In summary, the curves representing the dependence of $s_o t_3$ on the normalized sink magnitude s_o/s_c change quantitatively but not qualitatively with the substantial variations of ρ_s, r_s and cyclone intensity covered by the foregoing numerical experiments. While the effect becomes more subtle as r_s decreases toward ρ_s, the curves generally indicate transitions from relatively slow to fast intensification mechanisms as s_o increases beyond the neighborhood of the ideal critical value s_c. Forthcoming analysis [see sections 4.2.3 and 5] will shed more light on the fundamental differences between the subcritical and supercritical intensification mechanisms.

4.2.2 Cyclones with Azimuthally Drifting Mass Sinks

A distinct and exceptionally slow mode of intensification can be found in systems with azimuthally drifting mass sinks. Figure 6 shows $s_o t_3$ versus s_o/s_c for cyclones with AD mass sinks circulating around $\mathbf{x}_{c0}$ with an orbital radius of $r_s = 1$ and angular velocities ranging from $\Omega_s = 0.25$ to 0.75. The data cover systems with Fr=0.042, Ro=1.47, $\rho_s = 0.18$ [Fig. 6a]

and $\rho_s = 0.37$ [Fig. 6b]. Dashed reference curves are shown for similar systems with non-drifting (STI) mass sinks.

Regardless of the size and angular velocity of the AD mass sink, decreasing s_o/s_c from 2 toward subcritical values eventually leads to an abrupt departure of $s_o t_3$ from the dashed reference curve. The departure occurs at greater values of s_o/s_c as Ω_s increases toward unity. The departure marks a transition to a mode of intensification several times slower than the subcritical mode of systems with STI mass sinks. The exceptionally long intensification times are close to those for axisymmetric development when the mass sink component of S (in the disc at $\mathbf{x}_s$) is uniformly redistributed over the annulus defined by $r_s - \rho_s \leq r \leq r_s + \rho_s$, in which r is measured from the initial vortex center. The theory outlined in appendix C1 shows that the maximum of $\bar{v}$ in the symmetrized system stays within the annulus and triples in magnitude over the scaled time period $s_o t_3 = 147$ (35) when $\rho_s = 0.18$ (0.37), which is comparable to the largest value in Fig. 6a (6b). The preceding result suggests that giving the mass sink a sufficiently large azimuthal velocity, while lowering its magnitude to keep s_o/s_c fixed, can effectively transform the asymmetric system into a symmetric system with a rigid annular mass sink whose mean radius from the center of the vortex is close to r_s. Section 4.2.3 will verify that the asymmetric systems exhibiting exceptionally slow intensification resemble the symmetric system, in that the radius of maximum azimuthal velocity and the distance separating the circulating mass sink from the vortex center tend to maintain values near r_s; considerable deviations may occur but do not persist over time.

Note that increasing Ω_s toward unity while leaving s_o unchanged would simultaneously increase s_o/s_c toward infinity, since $s_c = 2|\bar{v}(r_s) - r_s\Omega_s|/\rho_s$ and $\bar{v}(r_s) = r_s = 1$ for systems with the AD mass sinks under present consideration. This fact together with Fig. 6 suggests that increasing Ω_s alone could either slow or accelerate intensification. Moreover, increasing Ω_s at constant s_o may result in nonmonotonic variation of t_3. For example, the small white circles in Fig. 6a show three simulations with $s_o = 4.34$, for which $s_o t_3$ changes from 36.6 to 130.8 to 11.5 as Ω_s increases from 0 to 0.5 to 0.75. That is to say, increasing Ω_s alone

changes a moderately fast subcritical mode of intensification (with $s_o/s_c = 0.4$) to a slower pseudo symmetric mode (with $s_o/s_c = 0.8$) to a rapid supercritical mode (with $s_o/s_c = 1.6$).

4.2.3 Structural Changes to the Cyclone During Supercritical and Subcritical Development

Distinct developmental pathways generally coincide with structural differences of the shallow-water cyclones at the end of the 3-fold intensification period ($t = t_3$). One basic structural parameter denoted r_m is the radius of maximal $\bar{v}$ in the vortex-centered reference frame, measured outside the assumed minimal core radius r_c of a mature hurricane. Another basic parameter is the distance between the centers of the mass sink and the vortex, given by $\ell \equiv |\mathbf{x}_s - \mathbf{x}_c|$. The values of r_m and ℓ at $t = t_3$ are respectively denoted by r_{m3} and ℓ_3.

Figure 7a shows a scatter plot of r_{m3} versus ℓ_3 for all previously considered systems having STI and AD mass sinks with $r_s = 1$ and $\rho_s = 0.18$. The white data correspond to systems with empirically supercritical mass sinks, defined as those for which $s_o t_3$ lies in close proximity to the small and roughly constant value found when s_o/s_c appreciably exceeds unity. That is to say, the white data account for the systems with $s_o t_3$ between 10.5 and 14.6. The grey data account for the systems with subcritical mass sinks and $s_o t_3$ between 23.5 and 40.7. The black data correspond to the very slowly developing systems with AD mass sinks and $s_o t_3$ between 128.4 and 167.2. All plotted data points satisfy the relation $|r_{m3} - \ell_3| \leq \rho_s$, meaning that the radius of maximum azimuthal velocity roughly corresponds to the nominal radius of deep convection (concentrated convergence) measured from the center of the vortex. On the other hand, each shaded data cluster (white, grey or black) is well separated from the other two.

The supercritical systems are distinguished by having $r_{m3} = r_c$ and $\ell_3 \lesssim \rho_s$. In other words, the inner core of the vortex relocates to the vicinity of the mass sink and dramatically contracts at some point before the vortex intensity triples in magnitude. The time series of the vortex parameters consistently indicate that the relocation occurs by the process of core

reformation.[6] Near $s_o t = 5$ or 6, depending on the cyclone strength, both r_m and ℓ abruptly drop to values less than ρ_s, and stay small for the remainder of the intensification period [Figs. 8a and 8b]. At the same transition time, there is an abrupt steepening of the time series of v_m, defined as the maximum of $\bar{v}$ for $r \geq r_c$ [Fig. 8c].

The systems with subcritical mass sinks belonging to the grey data set of Fig. 7a are distinguished by having middle-range values of r_{m3} and ℓ_3, each being larger than ρ_s but considerably smaller than the original radial length scale (unity) of the cyclone. Many of the time series for r_m and ℓ [Figs. 8d and 8e] show gradual decay with an intermediate slowdown period. Others show abrupt early drops in both r_m and ℓ, reflecting core reformation events. Following core reformation in this subgroup of subcritical systems with s_o relatively close to s_c, the vortex center drifts away from the mass sink (ℓ increases) and the radius of maximum azimuthal velocity (r_m) grows. The time series of v_m [Fig. 8f] abruptly steepens upon core reformation should such an event occur, but the steepening is shortly reduced. The intensification of v_m is otherwise relatively smooth.

The very slowly developing systems with AD mass sinks represented by the black data points in Fig. 7a are distinguished by having final values of r_m and ℓ that are fairly close to their original values of unity. The time series of the structural parameters [Figs. 8g-8i] show a few cases in which a reformed core of smaller scale temporarily dominates, but is later overtaken by the larger scale circulation. The thick dashed curve in Fig. 8i shows v_m for the symmetric analog system [appendix C1] whose mass sink is uniformly spread over the orbital annulus of width $2\rho_s$ centered at $r = 1$. The dashed curve agrees reasonably well with the bundle of solid curves. The foregoing result corroborates our previous suggestion that adding sufficient azimuthal drift to the mass sink while reducing s_o to maintain its ratio to s_c can effectively symmetrize development.

Figure 7b shows a scatter plot of r_{m3} versus ℓ_3 for all previously considered systems having STI and AD mass sinks with $r_s = 1$ and $\rho_s = 0.37$. The data points are again

[6] In this paper, we consider core reformation to occur when ℓ decreases by order unity over a time interval no greater than (commonly much less than) s_o^{-1}.

grouped into several shades corresponding to distinct intervals of the scaled intensification time $s_o t_3$. The white data account for systems with $s_o t_3$ between 4.4 and 6.3. The grey data account for systems with subcritical mass sinks and $s_o t_3$ between 7.4 and 10.5. The black data correspond to the slower developing systems with AD mass sinks and $s_o t_3$ between 27.9 and 36.9. As found for the cyclones with smaller mass sinks, ℓ_3 is positively correlated to r_{m3}. On the other hand, the two variables are not quite as closely matched. Moreover, the separation between the supercritical systems (white data) and the grey subcritical systems is less pronounced. The clearest distinguishing feature is that the grey values of r_{m3} generally exceed the minimal value r_c that is characteristically found in the cyclones with supercritical mass sinks. However, the grey values of ℓ_3 are generally within the upper bound (ρ_s) of the spectrum that is seen in supercritical systems. Notably, this means that the vortex centers of the grey subcritical systems eventually reach the mass sink. Time series of the structural parameters (not shown) are similar to those found for the three groups of systems with smaller mass sinks. A minor but notable difference is that r_m and ℓ tend to undergo smoother (but still very rapid) transitions during core reformation events.

4.2.4 Cyclones with Pulsating Mass Sinks

Consider next the intensification of cyclones with P mass sinks whose pulsation amplitudes are uniformly given by $s_p = 1.33 s_c$, and thus satisfy the condition $s_p/2 < s_c < s_p$. Figure 9a depicts the time-dependence of the sink magnitude $s(t)$ over the first wave period. The mass sink is subcritical until $t = t_c^-$, whereupon it becomes supercritical and maintains supercritical status until $t = t_c^+$.[7] The transition times are solutions to the equation $t_c^{\pm} = \tau_p \cos^{-1}\left(1 - 2s_c/s_p\right)/(2\pi)$. The width of the supercriticality interval $(t_c^+ - t_c^-)$ therefore increases from 0 to $\tau_p/2$ as s_p increases from s_c to $2s_c$.

[7]The instantaneous state of a pulsating mass sink is here called supercritical (subcritical) when $s > s_c$ ($s < s_c$), in which s_c is evaluated from the *initial* state of the cyclone. Bear in mind that this mathematical distinction loses some physical relevance if the cyclone intensifies appreciably before s surpasses s_c.

Figure 9b shows the variation of the scaled intensification time $s_c t_3$ (circles) with the scaled wave period $s_c \tau_p$ for systems with Fr=0.042, Ro=1.47, $r_s = 1$ and $\rho_s = 0.18$. The dashed horizontal reference line shows the intensification time of a system with the same parameters, but with a time independent (STI) mass sink whose magnitude s_o equals the subcritical time average ($s_p/2 = 0.67 s_c$) of the P mass sink magnitude $s(t)$. The lower and upper boundaries of the shaded wedge respectively correspond to $s_c t_c^-$ and $s_c t_c^+$. In other words, for a given value of the independent variable $s_c \tau_p$, the vertical extent of the shaded wedge spans the (scaled) time interval during the first wave period when $s(t)$ is supercritical.

For $s_c \tau_p$ of order unity or less, the intensification time is approximately that obtained when $s(t)$ is replaced with its subcritical time average. The intensification time then sharply drops into the supercriticality wedge as $s_c \tau_p$ increases from approximately 10 to 20. At this point, the supercriticality interval of the pulsation appears to be sufficiently long to permit the faster mode of intensification that is found in supercritical STI mass sinks. The fast mode of intensification continues to be triggered with growing delay (due to growing t_c^-) as $s_c \tau_p$ increases another order of magnitude. Note that when the delay becomes sufficiently large, the slow mode of intensification can substantially amplify v_m before s becomes supercritical.

4.3 Development of Cyclones Forced by Radially Drifting Mass Sinks

Let us now consider a cyclone with an RD mass sink initially located at the center of the vortex. The central question is whether the mass sink will escape the core of the vortex before major intensification. One might suppose that escape can occur only if the mass sink magnitude s_o is sufficiently small or its radial drift velocity $\dot{r}_s$ is sufficiently large. The following suggests that the quantitative condition for escape is linked to the subcriticality condition $s_o < s_c = 2\dot{r}_s/\rho_s$.

Figure 10 shows one of two time periods associated with a cyclone whose initially centered RD mass sink is characterized by $\rho_s = 0.37$. One time period (t_3) applies to cyclones that triple their intensity, as measured by v_m, before the mass sink separates from the vortex

center by a distance $\ell = 2$, corresponding to twice the initial radius of maximum velocity. To facilitate discussion, these cyclones are said to "fully develop." The fully developed cyclones are represented by shaded symbols. Different symbol shapes correspond to different settings for Fr, Ro and $\dot{r}_s$. Virtually all of the fully developing systems have mass sink magnitudes at or above the theoretical critical value s_c; the only minor exception is seen when the cyclone is relatively weak and $\dot{r}_s = 1$, in which case full development occurs down to $s_o = 0.75 s_c$. Moreover, all of the fully developing systems triple in strength over the short time period that is predicted by axisymmetric theory [appendix C2] and shown by the dashed horizontal line for systems with Ro=1.47. Variation of this line with Ro is hardly discernible over the present simulation set.

The other time period ($t_{\ell 2}$) is that required for the mass sink to separate a distance $\ell = 2$ from the vortex center, and applies to cyclones that fail to triple their intensity by then. Such cyclones are said to have underdeveloped end states. Underdeveloped cyclones are represented by white symbols. Their mass sink magnitudes are usually below s_c; an exceptional case of underdevelopment occurs at $s_o = s_c$ when the cyclone is relatively strong and $\dot{r}_s = 0.25$. Note that the plotted value of $s_o t_{\ell 2}$ generally exceeds the scaled time period $s_o t_{r2} \equiv 4 s_o / s_c \rho_s$ (the dashed diagonal line) required for the mass sink to reach a radius $r_s = 2$ from the *initial* vortex center $\mathbf{x}_{c0}$. The relation $t_{\ell 2} > t_{r2}$ results from the early, sometimes prolonged, attraction of the actual vortex center to the mass sink.

Figure 11 shows trajectories in ℓ-v_m phase space of cyclones that fully develop (solid curves) and cyclones that do not (dashed curves). The centers of cyclones that fully develop are seen to stay inside the supercritical mass sinks ($\ell \leq \rho_s = 0.37$) that enable the rapid 3-fold intensification process. The cyclones that fail to fully develop are seen to cease intensification once the distance ℓ between the subcritical mass sink and the vortex center surpasses ~ 0.5. For these cases, the smallest terminal value of v_m belongs to the system with $s_o/s_c = 0.25$, whereas the largest terminal value is shared by two systems with $s_o/s_c = 0.75$ and 1. The latter systems can be identified in Fig. 10 as those with the largest values of $s_o t_{\ell 2}$.

During the review of this paper, a number of simulations excluded from Table I were conducted with RD mass sinks distinctly having (1) $\rho_s = 0.18$ and $r_{s0} = 0$, or (2) $\rho_s = 0.37$ and $r_{s0} = 0.5$. Common system parameters were given by $\dot{r}_s = 0.5$, $\Omega_s = 0$, Fr=0.042 and Ro=1.47. Both groups of simulations were consistent with the foregoing results in demonstrating a transition from supercritical development to subcritical underdevelopment as the ratio of s_o to s_c decreased below a value near unity (not shown). In calculating this ratio for simulations in group 2, the working formula for the critical convergence was changed from $s_c = 2\dot{r}_s/\rho_s$ to $s_c = 2[\bar{v}^2(r_{s0}) + \dot{r}_s^2]^{1/2}/\rho_s$ so as to appropriately take into account the nonzero value of the azimuthal velocity field at the initial location of the mass sink.

One might speculate that the findings of this subsection offer some insight into the vulnerability of tropical cyclone development to progressive enhancement of vertical wind shear. Such speculation is based on the supposition that enhanced shear would act to increase tilt and thereby nudge the lower tropospheric convergence zone associated with deep convection farther away from the surface-center of the vortex. Although continual radial drift of the convergence zone and ultimate shutdown of development in a subcritical system would not be expected if the shear saturates at a moderate level, intensification would be expected to slow down if the convergence could not keep the vortex center relatively close [see Fig. 5].

5. Further Analysis of a Selected Subcritical System

The spinup of a supercritical system basically involves fluid with positive absolute vorticity continually converging toward a point of attraction in the mass sink with no chance of escape. Understanding the variability in details does not seem crucial, and is therefore set aside. There is also little motivation to elaborate on the exceptionally slow intensification of subcritical systems whose mass sinks have appreciable azimuthal drift. Such systems were shown to behave much like their symmetric counterparts whose mass sinks are uniformly spread over the orbital annulus. On the other hand, development of subcritical systems with

minimal or no azimuthal drift can be subtle and requires further discussion.

5.1 The Spinup of a Cyclone with a Subcritical STI Mass Sink

The following analysis pertains to a cyclone possessing a subcritical STI mass sink with $s_o = 0.33 s_c$, $\rho_s = 0.18$ and $r_s = 1$. The initial Froude and Rossby numbers are respectively given by Fr=0.042 and Ro=1.47. The behavior of the preceding system is considered typical of those in the "grey zone," i.e., those represented by the grey data in Fig. 7a.

Figure 12 depicts the evolution of the velocity and relative vorticity fields during the intensification period. Local convergence amplifies the vorticity of fluid entering the mass sink. Because the mass sink is subcritical, it allows this fluid to escape and continue along a broad quasi-circular path. The initial effect is a cyclonically circulating ribbon of enhanced vorticity emanating from the mass sink. Over time, the head of the ribbon returns to the vicinity of the mass sink, marking the formation of a vorticity annulus. Meanwhile, the cyclonic winds intensify and the radius of maximal $\bar{v}$ (the outer radius of the annulus) contracts. The contraction coincides with motion of the vortex center toward the mass sink. The concomitant emergence of mesovortices along the annulus seems attributable to a combination of the localized forcing within the mass sink and the general susceptibility of vorticity ribbons to roll-up instabilities [e.g., Schubert et al. 1999; Naylor and Schecter 2014].

Continual reduction of the distance ℓ between the centers of the vortex and the mass sink distinguishes subcritical systems in the grey zone (such as that considered here) from their slower developing counterparts with mass sinks that have appreciable azimuthal drift and maintain a large orbital radius. Appendix C1 provides evidence that a symmetrized system develops faster when the mass sink is closer to the vortex center. Such evidence suggests that faster development in the grey zone is closely linked to the continual reduction of ℓ.

If the cyclone were a point vortex in a setting with no planetary vorticity ($f = 0$), the time derivative of ℓ would equal the local velocity $u_{\rm snk}$ of the inflow toward $\mathbf{x}_s$ that is

generated by the mass sink [Eq. (5)]. An analytical expression for $u_{\rm snk}$ at low Froude number is readily obtained by integrating the relation $\ell^{-1}d(\ell u_{\rm snk})/d\ell = S/h_0$ [see Eq. (3)], resulting in $u_{\rm snk} = -(s_o\rho_s^2/2\ell)(1-\pi\ell^2/A_d)$ under the assumptions that $\ell \geq \rho_s$ and boundary effects are negligible. It follows from $d\ell/dt = u_{\rm snk}$ that

$$\ell = \left\{ \frac{A_d}{\pi} \left[1 - \left(1 - \frac{\pi\ell_0^2}{A_d} \right) \exp\left(\frac{\pi\rho_s^2 s_o (t-t_0)}{A_d} \right) \right] \right\}^{1/2}, \tag{15}$$

in which ℓ_0 is the value of ℓ at $t = t_0$. Figure 13a compares the actual time series of ℓ to solutions of the point vortex drift model [Eq. (15)] with $s_o t_0 = 0$ and 25. The model underestimates the early decay of ℓ and overestimates the late decay. Such inaccuracy is clearly reasonable given that the cyclone is not a point vortex and f is nonzero.

Moreover, under ordinary conditions, motion of the vortex center in a diabatic (or quasi-diabatic) system cannot be understood simply as an advective process. A clear counterexample is the abrupt change of location that follows core reformation in a supercritical system. Fundamentally, the vortex center $\mathbf{x}_c(t)$ moves because the azimuthal flow centered at the end point of the trajectory becomes stronger than the azimuthal flow centered at the starting point. Figures 13b and 13c illustrate the dynamics for the case at hand. The left and right r-t Hovmöller plots show the evolutions of $\bar{v}$ in the stationary coordinate systems centered at $\mathbf{x}_{c0} \equiv \mathbf{x}_c(0)$ and $\mathbf{x}_{c3} \equiv \mathbf{x}_c(t_3)$, respectively. By the end of the intensification period, the amplification of maximal $\bar{v}$ around $\mathbf{x}_{c3}$ far exceeds the modest amplification of $\bar{v}$ around $\mathbf{x}_{c0}$. Analysis of the former will follow a brief discussion of the pertinent theoretical framework.

5.2 Formulation of the Angular Momentum Budget

The equations governing the φ-averaged azimuthal velocity field (without friction) and height field are respectively

$$\frac{\partial \bar{v}}{\partial t} = -\bar{u}\bar{\eta} + \mathcal{E}_v \qquad \text{and} \tag{16a}$$

$$\frac{\partial \bar{h}}{\partial t} = -\frac{1}{r}\frac{\partial (r\bar{u}\bar{h})}{\partial r} + \mathcal{E}_h + \bar{S}, \tag{16b}$$

in which

$$\mathcal{E}_v \equiv -\overline{u'\zeta'} \quad \text{and} \quad \mathcal{E}_h \equiv -\frac{1}{r}\frac{\partial(r\overline{u'h'})}{\partial r} \tag{16c}$$

are the eddy forcings. Following standard practice, we have used an overbar (prime) to denote the azimuthal mean (asymmetric perturbation) of a fluid variable. Let us further assume that the $\bar{u}$ equation approximates to gradient balance,

$$\frac{\partial \bar{h}}{\partial r} = \mathrm{Fr}^2 \left(\frac{\bar{v}^2}{r} + \frac{\bar{v}}{\mathrm{Ro}} \right), \tag{16d}$$

which is solved under the assumption that $\bar{h} = h_0 = 1$ at $r = r_e \gg \max(1, r_s)$. Equations (16a)-(16d) apply to both stationary and translating reference frames.

A formula for the mean radial velocity consistent with maintenance of gradient balance during the vortex evolution is obtained by taking the partial time derivative of Eq. (16d), and replacing $\partial\bar{v}/\partial t$ and $\partial\bar{h}/\partial t$ with the right-hand sides of Eqs. (16a) and (16b). The result is the following shallow-water Sawyer-Eliassen (SE) equation [Smith 1981; Willoughby 1994]:

$$\frac{\partial^2 \mathcal{U}}{\partial r^2} - \frac{1}{r}\frac{\partial \mathcal{U}}{\partial r} - \mathrm{Fr}^2 \frac{\bar{\eta}\bar{\xi}}{\bar{h}} \mathcal{U} = \mathcal{F}_s + \mathcal{F}_{ev} + \mathcal{F}_{eh}, \tag{17a}$$

in which $\mathcal{U} \equiv r\bar{u}\bar{h}$, $\bar{\xi} \equiv 2\bar{v}/r + \mathrm{Ro}^{-1}$, and

$$\begin{aligned} \mathcal{F}_s &\equiv r\frac{\partial \bar{S}}{\partial r}, \\ \mathcal{F}_{ev} &\equiv -\mathrm{Fr}^2 r\bar{\xi}\mathcal{E}_v, \\ \mathcal{F}_{eh} &\equiv r\frac{\partial \mathcal{E}_h}{\partial r}. \end{aligned} \tag{17b}$$

The SE equation is supplemented herein with the boundary conditions $\mathcal{U} = 0$ at the origin and at the distant radius r_e. Note that as $\mathrm{Fr}^2 \to 0$, along with $h' \to 0$ and $\bar{h} \to h_0$, the SE equation becomes consistent with Eq. (3) in reducing to $r^{-1}\partial(r\bar{u})/\partial r = \bar{S}/h_0$. The preceding small Froude number formula for $\bar{u}$ is obtained by integrating the SE equation in r.

Because the SE equation is linear, we may write

$$\mathcal{U} = \sum_{\alpha\in\{s,ev,eh\}} \mathcal{U}_\alpha, \tag{18}$$

in which $\mathcal{U}_\alpha$ is the solution when keeping only $\mathcal{F}_\alpha$ on the right-hand side. Physically, $\mathcal{U}_\alpha$ represents a radial velocity field (times $r\bar{h}$) that would be required to maintain gradient-balance in response to the diabatic or eddy forcing associated with $\mathcal{F}_\alpha$ alone. Substituting $\bar{u} = \mathcal{U}/(r\bar{h})$ into Eq. (16a) and using Eq. (18) yields

$$\frac{\partial \bar{v}}{\partial t} = -\sum_{\alpha\in\{s,ev,eh\}} \bar{u}_\alpha \bar{\eta} \; + \; \mathcal{E}_v, \tag{19}$$

in which $\bar{u}_\alpha \equiv \mathcal{U}_\alpha/(r\bar{h})$. The angular momentum transport accounted for by $-\bar{u}_s\bar{\eta}$ would be the sole contributor to $\partial\bar{v}/\partial t$ in a system with symmetric diabatic forcing. For systems pertinent to the present study, asymmetric diabatic forcing creates eddies that add both indirect ($-\bar{u}_{ev}\bar{\eta} - \bar{u}_{eh}\bar{\eta}$) and direct ($\mathcal{E}_v$) contributions to the budget.

While the indirect contributions of eddy forcing are typically small, $\mathcal{E}_v$ can be significant and worthy of further analysis. To this end one may consider the following Helmholtz decomposition of the velocity field: $\mathbf{u} = \mathbf{u}_\chi + \mathbf{u}_\psi + \mathbf{u}_a$. The irrotational and nondivergent contributions are respectively given by $\mathbf{u}_\chi = \nabla\chi$ and $\mathbf{u}_\psi = \hat{\mathbf{z}}\times\nabla\psi$, in which $\nabla^2\chi = \nabla\cdot\mathbf{u}$ and $\nabla^2\psi = \zeta$. The preceding Poisson equations for the velocity potential χ and streamfunction ψ are solved herein over a square simulation domain with doubly periodic boundary conditions. The third component of the velocity field ($\mathbf{u}_a$) corresponds to the domain average of $\mathbf{u}$. Taking the Helmholtz decomposition into consideration, one may write

$$\mathcal{E}_v = -\overline{u'_\chi\zeta'} - \overline{u'_\psi\zeta'} - \overline{u_a\zeta'}. \tag{20}$$

Because u_a varies with the translational velocity of the reference frame, so too does $\mathcal{E}_v$. By contrast, the instantaneous value of $-\bar{u}\bar{\eta}$ depends only on the instantaneous center of the coordinate system.

781 *5.3 Analysis of the Intensification of a Cyclone with a Subcritical STI Mass Sink*

782

783 We are now in a position to analyze the spinup of the subcritical system of section 5.1
784 in a stationary coordinate system whose origin resides at $\mathbf{x}_{c3}$, and therefore coincides with
785 the vortex center at the end of the intensification period. Figure 14a shows the running
786 time integral of the right-hand side of Eq. (19) with initial conditions matching those of
787 the simulation. The result is virtually indistinguishable from the simulation output for
788 $\bar{v}$ [Fig. 13c], thus verifying the accuracy of the SE approximation for $\bar{u}$. Further investigation
789 has shown that the SE approximation for $\bar{u}$ is virtually indistinguishable from the solution
790 to the low Froude number equation, $r^{-1}\partial(r\bar{u})/\partial r = \bar{S}/h_0$. The foregoing result suggests that
791 $\bar{u}_s \gg \bar{u}_{ev}, \bar{u}_{eh}$, which has been duly verified. Equally important, the eddy forcing driven by
792 nondivergent winds ($-\overline{u'_\psi \zeta'}$) has been found to largely control the time integral of $\mathcal{E}_v$; other
793 contributions are relatively minor.

794 Figures 14b and 14c show the two principal contributions to the change of $\bar{v}$ over the
795 intensification period. The time integral of $-\bar{u}_s\bar{\eta}$ [Fig. 14b] alone would amplify the vortex
796 by roughly a factor of 6. Persistent damping by the primary eddy forcing implied by the
797 increasingly negative running time integral of $-\overline{u'_\psi \zeta'}$ [Fig. 14c] is crucial to reducing the
798 actual amplification factor to 3. While the negative eddy forcing has not been thoroughly
799 studied, one contributing factor could be the continual advection of localized sink-enhanced
800 vorticity out of the inner core centered at $\mathbf{x}_{c3}$, most apparent in the lower-left panel of Fig. 12.

It is instructive to compare the preceding angular momentum budget to that observed in the moving vortex-centered reference frame. Here too, it is found that the theoretical approximation of $\partial\bar{v}/\partial t$ [Eq. (19)] is excellent and $\bar{u}_s \gg \bar{u}_{ev}, \bar{u}_{eh}$. Figure 15a shows the evolution of $\bar{v}$ taken directly from the simulation. The radius of maximal $\bar{v}$ stays near but outside the contracting radial coordinate (ℓ) of the mass sink. Figure 15b shows the partially reconstructed velocity field

$$\bar{v}_s \equiv \bar{v}(r,0) - \int_0^t \bar{u}_s\bar{\eta}\, dt$$

obtained when only the influx of absolute vorticity driven by $\bar{u}_s \approx \bar{u}$ contributes. The velocity boost associated with $-\bar{u}_s\bar{\eta}$ is smaller than its counterpart in the stationary coordinate system considered previously, but sufficient to triple the peak value of $\bar{v}$. Instead of broadly countering the intensification induced by $-\bar{u}_s\bar{\eta}$, the cumulative effect of the eddy forcing is to shift the peak of $\bar{v}$ from $r = 0.58$ to 0.42. As before, the time integral of $-\overline{u'_\psi\zeta'}$ [Fig. 15c] tends to be larger than the time integrals of other contributions to $\mathcal{E}_v$, but the combined influence of $-\overline{u'_\chi\zeta'}$ and $-\overline{u_a\zeta'}$ is appreciable [Fig. 15d].

6. Discussion

6.1 Pathway of Tropical Cyclone Development

The theory of tropical cyclone intensification has a long and venerable history [see Montgomery and Smith 2014; Emanuel 2018]. The present study is among others suggesting that a complete theory must address which of several distinct pathways of intensification is most likely to operate under specific conditions, especially during the early stages of development when strong asymmetries may exist [cf. Nicholls and Montgomery 2013]. The shallow-water model hints that the prevailing pathway may depend on whether conditions facilitate or hinder the emergence and maintenance of a convergence zone of supercritical intensity. It is therefore of interest to ask whether a supercritical convergence zone can actually exist in a real tropical cyclone.

The following range of estimates for s_c suggest that a supercritical convergence zone is within the realm of possibilities. Consider an incipient tropical cyclone with a mean azimuthal velocity $V_{\rm TC}$ of 10-20 m s^{-1} in the vicinity of an off-center convergence zone associated with vigorous deep convection.[8] Suppose that the convergence zone has an effective radius ρ_s of 50-75 km, and propagates with azimuthal velocity $\epsilon V_{\rm TC}$. Letting ϵ vary from 0 to 0.7 would yield $s_c = 2V_{\rm TC}(1-\epsilon)/\rho_s = 8\times10^{-5} - 8\times10^{-4}$ s^{-1}. The smallest estimate of

[8]The asterisk denoting dimensional variables elsewhere is dropped for the present discussion.

s_c is obtained from the lower limit of $V_{\rm TC}$, the upper limit of ϵ, and the upper limit of ρ_s; the largest estimate is obtained from the opposite limits. One might imagine a number of other reasonable parameter variations that give similar results. Taking the smallest estimate for s_c and only a slightly greater value for the average intensity s_o of the convergence zone, the time scale s_o^{-1} for supercritical dynamics to start having an impact would be approximately 3.5 h. Even this upper-end value for the time scale seems physically sound in falling within the reported range of achievable lifetimes for "extreme convection" in oceanic tropical weather systems [e.g., Gray 1998]. Moreover, an average intensity s_o exceeding the smallest estimate of s_c seems plausible based in part on documented studies of developing systems simulated with cloud resolving models [e.g., Chen et al. 2018]. That being said, the actual probability of pairing s_o with smaller s_c in nature is unknown at this time.

Whether the shallow-water condition for supercriticality ($s_o > s_c$) would really enable core reformation and rapid intensification in a tropical cyclone is another unresolved issue. The answer is presently unclear, not least because the shallow-water model neglects three-dimensional processes that generally complicate the flow within a moist-convective convergence zone. Moreover, the shallow-water model considered herein neglects frictional dissipation of angular momentum. Such neglect would seem unjustifiable when the convergence zone does not extend far above the frictional boundary layer. The present shallow-water model also neglects modifications to a natural convergence zone that may occur as friction and other factors influencing convection change after a potential core reformation process begins. Further study with cloud resolving simulations will be necessary to gain a firmer understanding of the qualitative applicability of shallow-water theory in its present form.

6.2 Symmetric versus Asymmetric Forcing

The findings of this study suggest that symmetrization of an off-center mass sink in a shallow-water cyclone commonly slows down the intensification process.[9] Such a result may seem

[9]Compare the small values of $s_o t_3$ given by filled circles in Fig. 4a (4b) to the large minimum of $s_o t_\#$ for $r_s = 1$ in Fig. C1a (C1b). Note that the aforementioned minimum of $s_o t_\#$ is the semi-analytical prediction for $s_o t_3$ in the symmetrized system.

at odds with the conventional view that symmetric convection facilitates the development of a tropical cyclone. Therefore, it is important to clarify what has actually been shown. *In the present context,* symmetrization constrains the distance between the mass sink and the vortex center to the initial value of ℓ. The asymmetric system has no such constraint, and (when Ω_s and $\dot{r}_s$ are minimal) permits the reduction of ℓ to values at which the symmetric component of the mass sink can more rapidly accelerate $\bar{v}$ in the vortex-centered reference frame. In axisymmetric tropical cyclone models where convection is dynamically coupled to the vortex structure, the mean radius of the main updraft (effective annular mass sink) generally contracts during development. Such contraction may allow symmetric pathways of tropical cyclone intensification to occur faster than asymmetric pathways of spinup resembling those considered herein.

Note further that the tendency of an asymmetrically forced shallow-water system to intensify faster than its symmetric counterpart with ℓ fixed to its initial value does not imply that the attendant eddy forcing of $\bar{v}$ has a major positive role in the amplification of v_m. Such was evident from the analysis of section 5 pertaining to a selected subcritical system with an STI mass sink that developed roughly four times faster than its symmetric counterpart. In a stationary coordinate system centered where $\mathbf{x}_c$ was located at the end of the intensification period, asymmetric eddy forcing strongly opposed the primary positive spinup tendency associated with the inflow of angular momentum induced by the symmetric component of the mass sink. In the moving vortex-centered reference frame, asymmetric eddy forcing appeared to have a relatively modest role in modulating the symmetrically amplified distribution of $\bar{v}$. Thus, the present results do not contradict the common view that the symmetric component of diabatic forcing within a tropical cyclone should provide the dominant positive contribution to the intensification of $\bar{v}$ [e.g., Nolan and Grasso 2003; Nolan et al. 2007].[10]

[10]Bear in mind that angular momentum transport by asymmetric eddies can be fairly complex in real-world or realistically simulated tropical cyclones [e.g., Nguyen et al. 2008; Persing et al. 2013; SM20]. There is no intention to suggest that the present findings on eddy transport in a simplified shallow-water simulation should qualitatively apply to all conceivable circumstances in nature.

7. Summary and Conclusions

This paper has examined the evolution of a shallow-water cyclone that contains an off-center convergence zone induced by a mass sink. Study of such a basic system was motivated by its possible relevance to the development of a misaligned tropical cyclone, in which convergence associated with deep convection is commonly enhanced in the downtilt sector of the lower tropospheric vortex. The pathway of vortex intensification was shown to depend on whether the magnitude of convergence generated by the mass sink exceeds a critical value $s_c = 2V_l/\rho_s$, in which ρ_s is the radial size of the mass sink, and V_l is the magnitude of the local vector-difference between the broader cyclonic velocity field and the drift velocity of the mass sink. Figure 16 illustrates some essential differences between the asymmetric pathways of intensification found to result from convergence above and below the critical value. Convergence exceeding s_c traps fluid undergoing vorticity amplification within the mass sink, whereas convergence less than s_c allows the fluid to escape. Consequently, supercritical convergence in our simulations generally enabled core reformation in the vicinity of the mass sink [Fig. 16a] followed by rapid intensification of the new and smaller core. Subcritical convergence generally coincided with a slower and more subtle spinup mechanism.

Systems possessing stationary time independent (STI) mass sinks of subcritical magnitude intensified through a process during which vorticity enhanced by the mass sink recirculates and the vortex center $\mathbf{x}_c$ gradually drifts toward the sink center $\mathbf{x}_s$ [Figs. 16b and 12]. In these and all other systems, contraction of the distance ℓ between the centers of the vortex and the mass sink coincided with contraction of the radius of maximum azimuthal velocity r_m. In a case study selected for detailed examination, the drift of $\mathbf{x}_c$ toward $\mathbf{x}_s$ did not closely follow the path predicted by a simplified model in which the extended cyclone was reduced to a point vortex passively drawn into the mass sink. Such a discrepancy was to be expected, not least because of continual vorticity production within the mass sink. The intensification of the maximum φ-averaged azimuthal velocity v_m was analyzed in the

moving vortex-centered reference frame, and in a stationary reference frame centered where $\mathbf{x}_c$ resides at the end of the intensification period. In both cases, the influx of absolute vorticity driven by the symmetric component of the sink-induced radial velocity field ($\bar{u}_s$) provided the dominant positive contribution to the intensification of v_m. Eddy forcing had a modulating influence in the vortex-centered reference frame, and a strongly negative influence in the stationary reference frame. Similar to the behavior of symmetric systems [Fig. 16c], increasing/decreasing the initial distance between an STI mass sink and $\mathbf{x}_c$ lengthened/shortened the intensification period.

Giving the mass sink sufficient azimuthal velocity ($r_s\Omega_s$), while simultaneously decreasing the magnitude s_o of the sink-induced convergence to conserve its ratio to s_c, revealed a much slower mode of intensification. The slower mode featured minimal long-term decay of ℓ, and a time series for v_m resembling that of a symmetric system in which the mass sink is uniformly spread over its orbital annulus. Transitions to the slower mode of intensification were found when starting from either subcritical or slightly supercritical systems whose mass sinks were stationary. Increasing Ω_s from zero *while keeping* s_o *constant* can ultimately change a subcritical system with a moderately paced asymmetric mode of intensification to a supercritical system with a much faster mode by reducing s_c. However, as shown by an illustrative example, the effectively symmetric slowest mode of intensification can occur in an intermediate frequency band.

Allowing the mass sink to pulsate adds another dimension to the evolution of a shallow-water cyclone. A subsection of the present study examined stationary, pulsating mass sinks generating convergence with a peak value s_p between s_c and $2s_c$. For a pulsation period τ_p substantially less than $1/s_c$— the time scale for the broader cyclone to advect a fluid parcel across the mass sink —the cyclone slowly intensified as though it possessed a subcritical STI mass sink generating steady convergence of magnitude $s_p/2 < s_c$. Increasing $s_c\tau_p$ substantially above unity allowed core reformation and rapid intensification to occur during the first supercritical phase of the pulsation. A similar scenario unfolded with increasing delay as

$s_c\tau_p$ was taken up to values of order 100.

A distinct set of numerical simulations considered the behavior of a shallow-water cyclone with a radially drifting (non-pulsating) mass sink starting at the center of the vortex. As usual, the behavior depended on whether the magnitude of sink-induced convergence s_o exceeded the critical value s_c, here calculated with V_l equaling the radial drift velocity $\dot{r}_s$. Subcritical mass sinks with $s_o < s_c$ generally escaped the trailing core of the cyclone before completion of the intensification process. By contrast, supercriticality ($s_o > s_c$) generally guaranteed rapid intensification and full development.

Acknowledgments and Data Statement: The author thanks three anonymous reviewers for their constructive comments. This work was supported by the National Science Foundation under grant AGS-1743854. The cloud resolving simulation shown in appendix A was made possible by a computing allocation granted by the National Center for Atmospheric Research [doi:10.5065/D6RX99HX]. Data is presently obtainable from the author upon request.

Appendix A: Asymmetric Convergence in a Simulated Tropical Cyclone

The main purpose of this appendix is to illustrate the localized off-center convergence in the lower troposphere said to be common in cloud resolving simulations of misaligned tropical cyclones. Figures A1a-A1c show a 6-h time-averaged view of a misaligned tropical cyclone simulated by Schecter and Menelaou [SM20] prior to the onset of rapid intensification. Configurational details of the simulation— named DSPD-X400Z5 —can be found in the foregoing reference. Consistent with statements in the main text, convergence of the horizontal velocity field is clearly enhanced near the off-center focal point of deep convection in the downtilt sector of the lower tropospheric vortex [Fig. A1a]. Although patches of divergence exist within the vortex core, their subdominance at this time is evident in that the irrotational wind over the entire vortex core streams into the region of enhanced convergence.

Note also that the principal region of convection and convergence occurs near the radius of maximum cyclonic velocity [Fig. A1b]. Qualitative aspects of the preceding scenario seem fairly normal throughout the early and intermediate stages of development of the system at hand. Another nice illustration of concentrated off-center lower tropospheric convergence in a more realistically simulated system can be found in Fig. 4 of Chen et al. [2018].

While not an explicit part of our shallow-water model, the moisture dynamics regulating deep convection and the associated lower tropospheric convergence merits some discussion. Figure A1c offers some insight into the moisture dynamics involved in maintaining asymmetric off-center convection in the tropical cyclone under present consideration. Convection downtilt of the surface-center of rotation is seemingly supported by an incoming stream of boundary layer air possessing moderately enhanced equivalent potential temperature (θ_e). The relatively high θ_e inflow appears to come partly from the outer vortex and partly from recirculating air in the core. Oceanic surface fluxes presumably help the recirculating air recover from exposure to any low θ_e downdrafts that may be connected to precipitation. The uptilt sector of the vortex is distinguished in part by having low humidity in the lower-middle troposphere, which among other possibilities may increase the negative feedback of entrainment on any local attempt to establish vigorous deep convection. Two factors that can contribute to low humidity uptilt are subsidence and ventilation by the horizontal winds of the middle tropospheric circulation [SM20].

Figures A1d and A1e verify that downtilt localization of the convergence zone near the radius of maximum wind speed is a persistent feature of the tropical cyclone under present consideration. The depicted 65-h time frame covers a period after genesis and before the onset of rapid intensification. The plotted convergence profiles are defined by

$$\mathcal{M}_r(r_*, t_*) \equiv - \langle r_* \nabla_* \cdot \mathbf{u}_* \rangle_{\varphi z} \quad \text{and} \quad \mathcal{M}_\varphi(\varphi, t_*) \equiv - \langle r_* \nabla_* \cdot \mathbf{u}_* \rangle_{rz} \,, \tag{A1}$$

in which r_* is the (dimensional) radius and φ is the azimuth in a surface vortex centered polar coordinate system. The operator $\langle \ldots \rangle_{\varphi z}$ in the definition of $\mathcal{M}_r$ denotes an average

over the full azimuthal circuit and the vertical interval $0 < z_* < 3$ km, in which z_* is the height above sea-level. In the Boussinesq approximation, where $-\nabla_* \cdot \mathbf{u}_* = \partial w_*/\partial z_*$, the integral of $\mathcal{M}_r$ over an arbitrary radial interval is directly proportional to the net upward mass current at $z_* = 3$ km on the annulus spanning that interval. It is seen that $\mathcal{M}_r$ stays peaked near the dashed curve tracing the radius of maximum wind during much of the evolution. The operator $\langle \ldots \rangle_{rz}$ in the definition of $\mathcal{M}_\varphi$ denotes an average over the radial interval $0 < r_* < 200$ km and the vertical interval $0 < z_* < 3$ km. In the Boussinesq approximation, the integral of $\mathcal{M}_\varphi$ over an arbitrary interval of φ is proportional to the net upward mass current at $z_* = 3$ km on the corresponding sector of a surface vortex centered disc with a radius of 200 km. It is seen that $\mathcal{M}_\varphi$ stays fairly concentrated near the white curve that traces the orientation angle of the tilt vector, which by definition points from the surface center to the middle tropospheric center of rotation.

Figure A1f shows the evolution of the φ-averaged azimuthal velocity near the surface of the tropical cyclone in the surface vortex centered reference frame. The absence of any abrupt change to the slow intensification during the depicted time interval is similar to what may be expected for a subcritical shallow-water system [see sections 3 and 4]. Subcritical behavior of a system whose convergence zone of radius ρ_{s*} has a small drift velocity relative to the local azimuthal velocity v_* is consistent with $-(\nabla_* \cdot \mathbf{u}_*)\rho_{s*}/2v_*$ having a characteristic value less than unity in the convergence zone. A characteristic value of order one-tenth is readily gleaned from Figs. A1a and A1b. Section 6.1 discusses the possibility of other asymmetric tropical cyclones behaving like supercritical shallow-water systems.

Appendix B: Computational Parameters

The computational parameters of the numerical model are defined in appendix C of Schecter and Montgomery [2006], and are listed in Table II. Briefly stated, L_{fg} (L_{cg}) denotes the full length of the inner fine grid (outer coarse grid), δx (ΔX) denotes the fine (coarse)

grid spacing, δt denotes the time step, $r_{\rm spng}$ ($\delta r_{\rm spng}$) denotes the inner radius (edge width) of the peripheral sponge ring, β denotes the momentum damping rate associated with the sponge-ring, and $\nu_{\rm fg}$ denotes the fourth-order hyperdiffusion coefficient on the fine grid. The hyperdiffusion coefficient on the coarse grid is given by $\nu_{\rm cg} = (\Delta X/\delta x)^4 \nu_{\rm fg}$. All tabulated values are nondimensionalized using L and LU^{-1} as the characteristic scales, in which L and U are defined in the last paragraph of section 2.1. For example, $\delta x = \delta x_*/L$ and $\delta t = U\delta t_*/L$, in which the asterisk as usual denotes a dimensional version of the variable.

Appendix C: Axisymmetric Development

C.1 Cyclones with Annular Mass Sinks

This appendix discusses the behavior of an azimuthally symmetric analog of an asymmetrically forced cyclone. Both systems are assumed to have the same initial distribution of $\bar{v}$, given by the right-hand side of Eq. (9). The forcing term in the continuity equation of the asymmetric system is given by S in Eq. (5). The mass sink in S is assumed to have a constant value of r_s (greater than ρ_s) and no pulsation ($s_p = 0$). The symmetric system is obtained by transforming the mass sink component of S from an off-center circular disc to a uniform distribution within an annulus defined by $r_- \le r \le r_+$, in which $r_\pm \equiv r_s \pm \rho_s$ and r is measured from $\mathbf{x}_{c0}$. The transformed forcing term is denoted $S_{\rm sym}$ and given by

$$\frac{S_{\rm sym}(r)}{h_0} = -\frac{s_o \rho_s^2}{r_+^2 - r_-^2}\Theta(r - r_-)\Theta(r_+ - r) + \frac{s_o \pi \rho_s^2}{A_d}\Theta(\sqrt{A_d/\pi} - r). \tag{C1}$$

Equation (C1) guarantees that

$$\int_A S_{\rm sym} dA = \int_A S dA, \tag{C2}$$

in which the area A of integration can be (1) any circular disc of radius r less than r_-, (2)

any circular disc of radius r between r_+ and $\sqrt{A_d/\pi}$, or (3) the annular region defined by $r_- \leq r \leq r_+$. Thus, the symmetric and asymmetric systems pump mass into the shallow-water layer at equivalent rates between any two radii that are both in region 1 or both in region 2. Moreover, the two systems pump mass out of the principal annular sink region at the same rate.

The time scale for symmetric intensification depends partly on the speed at which the radial velocity field advects angular momentum inward from the periphery of the cyclone. As usual, we will consider the regime of asymptotically small Froude numbers to permit the use of Eq (3). Integrating the aforementioned equation for the divergence of radial velocity in the symmetric system yields

$$u_{\rm sym}(r) = \frac{s_o \pi \rho_s^2 r}{2A_d} - \frac{s_o \rho_s^2}{2r} \times \begin{cases} 0 & r \leq r_- \\ (r^2 - r_-^2)/(r_+^2 - r_-^2) & r_- < r < r_+ \\ 1 & r \geq r_+, \end{cases} \tag{C3}$$

under the assumption that $r \leq \sqrt{A_d/\pi}$.

Conservation of absolute angular momentum in the symmetric system can be expressed as the following equation for the symmetric azimuthal velocity field:

$$r v_{\rm sym}(r,t) + \frac{r^2}{2{\rm Ro}} = r_o v_{\rm sym}(r_o, 0) + \frac{r_o^2}{2{\rm Ro}}, \tag{C4}$$

in which $r_o(r,t)$ is the initial radius of the fluid ring having radius r at time t. A formula for r_o is found by solving the equation $\partial r_o/\partial t = -u_{\rm sym}(r_o)$ with the boundary condition $r_o(r,0) = r$. For values of r beyond the radius very close to r_- where $u_{\rm sym}$ becomes negative, and for values of t sufficiently large to ensure that $r_o > r_+$, one finds that

$$r_o^2(r,t) = \frac{A_d}{\pi}\left[1 - \left(1 - \frac{\pi r_>^2}{A_d}\right)\left(\frac{\sigma r_+^2 - r_-^2}{\sigma r_<^2 - r_-^2}\right)^{\mu} \exp\left(\frac{-\pi \rho_s^2 s_o t}{A_d}\right)\right], \tag{C5}$$

in which $r_>$ ($r_<$) is the greater (lesser) of r_+ and r, $\sigma \equiv 1 - \pi(r_+^2 - r_-^2)/A_d$ and $\mu \equiv$

$\pi(r_+^2 - r_-^2)/(\sigma A_d)$. Note that for $r \geq r_+$ and $\pi\rho_s^2 s_o t/A_d \ll 1$, Eq. (C5) simplifies to $r_o^2 \sim r^2 + \rho_s^2\,(1 - \pi r^2/A_d)\,s_o t$.

The time at which $v_{\rm sym}$ reaches a threshold $v_\#$ at a specific radius r within or outside the principal negative annulus of the mass sink is found by numerically solving Eq. (C4) for t after replacing $v_{\rm sym}(r,t)$ with $v_\#$ and r_o with the right-hand side of Eq. (C5). Let us denote the solution by $t_\#(r)$. Figure C1a shows $s_o t_\#$ versus r for the case in which $v_\# = 3$, or thrice the initial maximum velocity of the vortex. Different curves correspond to systems whose mass sinks have different values of r_s ranging from 0.33 to 1.67; in all cases, $\rho_s = 0.18$. Each curve begins at a radius slightly greater than $r_-/[1 - \pi(r_+^2 - r_-^2)/A_d]^{1/2}$, where $u_{\rm sym} = 0$ and $v_{\rm sym}$ remains constant over time according to Eq. (16a) with $\mathcal{E}_v = 0$. In general, $v_{\rm sym}$ first reaches $v_\#$ ($t_\#$ is minimized) at a radius less than r_s, but the velocity at r_s achieves the same milestone shortly thereafter. Note also that increasing r_s increases the minimum time required for $v_{\rm sym}$ to reach $v_\#$. Figure C1b demonstrates that the radial dependence of $s_o t_\#$ is qualitatively the same when $\rho_s = 0.37$.

C.2 Cyclones with Centered Circular Mass Sinks

Cyclones whose mass sinks are parameterized by Eq. (5) with $r_s = 0$ are azimuthally symmetric without modification. As before, one may substitute a formula for $r_o(r,t)$ into Eq. (C4) and solve for the time t at which $v_{\rm sym}$ at r on the left-hand side equals a specific threshold. The appropriate formula is given by

$$r_o^2(r,t) = \frac{A_d}{\pi}\left[1 - \left(1 - \frac{\pi r_>^2}{A_d}\right)\left(\frac{\rho_s}{r_<}\right)^{2/[A_d/(\pi\rho_s^2)-1]} \exp\left(\frac{-\pi\rho_s^2 s_o t}{A_d}\right)\right], \tag{C6}$$

in which $r_>$ ($r_<$) is the greater (lesser) of ρ_s and r. The preceding equation is valid for any r, but assumes $r_o > \rho_s$. The values of t_3 producing the dashed lines in Fig. 5 correspond to the solutions of Eqs. (C4) and (C6) for t with $v_{\rm sym}(r,t) \to 3$ and $r \to r_c < \rho_s$.

References

Chen, X., Y. Wang, J. Fang, and M. Xue, 2018: A numerical study on rapid intensification of Typhoon Vicente (2012) in the South China Sea. Part II: Roles of inner-core processes. *J. Atmos. Sci.*, **75**, 235-255.

Emanuel, K., 2018: 100 years of progress in tropical cyclone research. *Meteor. Monographs*, **59**, 15.1-68.

Enagonio, J., and M.T. Montgomery, 2001: Tropical cyclogenesis via convectively forced Rossby waves in a shallow-water primitive equation model. *J. Atmos. Sci.*, **58**, 685-706.

Gray, W.M., 1998: The formation of tropical cyclones. *Meteor. Atmos. Phys.*, **67**, 37-69.

Hendricks, E.A., W.H. Schubert, Y.-h. Chen, H.-C. Kuo, and M.S. Peng, 2014: Hurricane eyewall evolution in a forced shallow water model. *J. Atmos. Sci.*, **71**, 1623-1643.

Lahaye, N., and V. Zeitlin, 2016. Understanding instabilities of tropical cyclones and their evolution with a moist convective rotating shallow-water model. *J. Atmos. Sci.*, **73**, 505-523.

Molinari, J., and D. Vollaro, 2010: Rapid intensification of a sheared tropical storm. *Mon. Wea. Rev.*, **138**, 3869-3885.

Montgomery, M.T., R.K. Smith, 2014: Paradigms for tropical cyclone intensification. *Aust. Meteor. Ocean. Journ.*, **64**, 37-66.

Naylor, J., and D.A. Schecter, 2014: Evaluation of the impact of moist convection on the development of asymmetric inner core instabilities in simulated tropical cyclones. *J. Adv. Model. Earth Syst.*, **6**, 1027-1048.

Nicholls, M.E., and M.T. Montgomery, 2013: An examination of two pathways to tropical cyclogenesis occurring in idealized simulations with a cloud-resolving numerical model. *Atmos. Chem. Phys.*, **13**, 5999-6022.

Nguyen, L.T., and J. Molinari, 2015: Simulation of the downshear reformation of a tropical cyclone. *J. Atmos. Sci.*, **72**, 4529-4551.

Nguyen, L.T., R.F. Rogers, and P.D. Reasor, 2017: Thermodynamic and kinematic influences on precipitation symmetry in sheared tropical cyclones: Bertha and Cristobal (2014). *Mon. Wea. Rev.*, **145**, 4423-4446.

Nguyen, S.V., R.K. Smith, and M.T. Montgomery, 2008: Tropical-cyclone intensification and predictability in three dimensions. *Q. J. Roy. Meteor. Soc.*, **134**, 563-582.

Nolan, D.S., and L.D. Grasso, 2003: Nonhydrostatic, three-dimensional perturbations to balanced, hurricane-like vortices. Part II: Symmetric response and nonlinear simulations. *J. Atmos. Sci.*, **60**, 2717-2745.

Nolan, D.S., Y. Moon and D.P. Stern, 2007. Tropical cyclone intensification from asymmetric convection: Energetics and efficiency. *J. Atmos. Sci.*, **64**, 3377-3405.

Ooyama, K., 1969: Numerical simulation of the life cycle of tropical cyclones. *J. Atmos. Sci.*, **26**, 3-40.

Persing, J., M.T. Montgomery, J.C. McWilliams, and R.K. Smith, 2013: Asymmetric and axisymmetric dynamics of tropical cyclones. *Atmos. Chem. Phys.*, **13**, 12299-12341.

Rappin, E.D. and D.S. Nolan, 2012: The effect of vertical shear orientation on tropical cyclogenesis. *Q. J. R. Meteorol. Soc.*, **138**, 1035-1054.

Reasor, P.D., and M.T. Montgomery, 2015: Evaluation of a heuristic model for tropical cyclone resilience. *J. Atmos. Sci.*, **72**, 1765-1782.

Rios-Berrios, R., C.A. Davis, and R.D. Torn, 2018: A hypothesis for the intensification of tropical cyclones under moderate vertical wind shear. *J. Atmos. Sci.*, **75**, 4149-4173.

Rostami, M., and V. Zeitlin, 2018: An improved moist-convective rotating shallow-water model and its application to instabilities of hurricane-like vortices. *Q. J. Roy. Meteor. Soc.*, **144**, 1450-1462.

Rozoff, C.M., J.P. Kossin, W.H. Schubert, and P.J. Mulero, 2009: Internal control of hurricane intensity variability: The dual nature of potential vorticity mixing. *J. Atmos. Sci.*, **66**, 133-147.

Sadourny, R., 1975: The dynamics of finite-difference models of the shallow-water equations. *J. Atmos. Sci.*, **32**, 680-689.

Schecter, D.A., and M. T. Montgomery, 2003: On the symmetrization rate of an intense geophysical vortex. *Dyn. Atmos. Oceans*, **37**, 55-88.

Schecter, D.A., and M.T. Montgomery, 2006: Conditions that inhibit the spontaneous radiation of spiral inertia-gravity waves from an intense mesoscale cyclone. *J. Atmos. Sci.*, **63**, 435-456.

Schecter, D.A., 2011: Evaluation of a reduced model for investigating hurricane formation from turbulence. *Q. J. Roy. Meteor. Soc.*, **137**, 155-178.

Schecter, D.A., 2018: On the instabilities of tropical cyclones generated by cloud resolving models. *Tellus A*, **70**, 1-30.

Schecter, D.A., and K. Menelaou, 2020: Development of a misaligned tropical cyclone. *J. Atmos. Sci.*, **77**, 79-111. doi:10.1175/JAS-D-19-0074.1.

Schubert, W.H., M.T. Montgomery, R.K. Taft, T.A. Guinn, S.R. Fulton, J.P. Kossin, and J.P. Edwards, 1999: Polygonal eyewalls, asymmetric eye contraction, and potential vorticity mixing in hurricanes. *J. Atmos. Sci.*, **56**, 1197-1223.

Schubert, W.H., C.J. Slocum and R.K. Taft, 2016: Forced, balanced model of tropical cyclone intensification. *J. Meteor. Soc. Japan, Ser. II,* **94**, 119-135.

Smith, R.K., 1981: The cyclostrophic adjustment of vortices with application to tropical cyclone modification. *J. Atmos. Sci.*, **38**, 2021-2030.

Tao, D., and F. Zhang, 2014: Effect of environmental shear, sea-surface temperature, and ambient moisture on the formation and predictability of tropical cyclones: An ensemble-mean perspective. *J. Adv. Model. Earth Syst.*, **6**, 384-404.

Willoughby, H.E., 1994: Nonlinear motion of a shallow water barotropic vortex. *J. Atmos. Sci.*, **51**, 3722-3744.

Zehnder, J.A., 2001: A comparison of convergence- and surface-flux-based convective parameterizations with applications to tropical cyclogenesis. *J. Atmos. Sci.*, **58**, 283-301.

sink type	s_o/s_c	s_p/s_c, $s_c\tau_p$	Ω_s	$\dot{r}_s$	r_{s0}	ρ_s	Fr	Ro
STI	0.33-2.0	0, —	0	0	0.38-2.17	0.18-0.37	0.042-0.084	1.47-2.95
AD	0.33-2.0	0, —	0.25-0.75	0	1.0	0.18-0.37	0.042	1.47
RD	0.25-2.0	0, —	0	0.25-1.0	0	0.37	0.021-0.084	0.74-2.95
P	0	1.33, 0.2-150	0	0	1.0	0.18	0.042	1.47

TABLE I. Physical parameters for simulations categorized by sink type.

parameter	values
$L_{\rm fg}$	5.97
$L_{\rm cg}$	19.6
$\delta x \times 10^3$	9.21
$\Delta X \times 10^3$	55.3
$\delta t \times 10^4$	1.84, 3.68, 7.37
$r_{\rm spng}$	8.84
$\delta r_{\rm spng}$	0.37
β	90.5, 45.3, 22.6
$\nu_{\rm fg} \times 10^8$	4.00, 2.00, 1.00

TABLE II. Nondimensional values of various computational parameters. From left to right, comma-separated values correspond to simulations initialized with (Fr,Ro) = (0.021,0.74), (0.042,1.47), and (0.084,2.95).

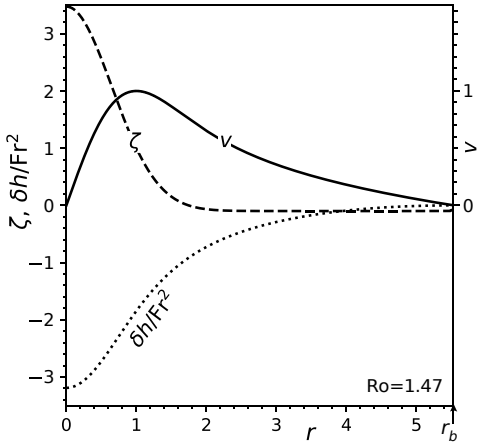

Figure 1: Relative vorticity (ζ), azimuthal velocity (v) and height anomaly ($\delta h \equiv h - 1$) of the initial axisymmetric vortex. The height anomaly is computed with Ro=1.47 and divided by Fr^2 so as not to depend on the Froude number.

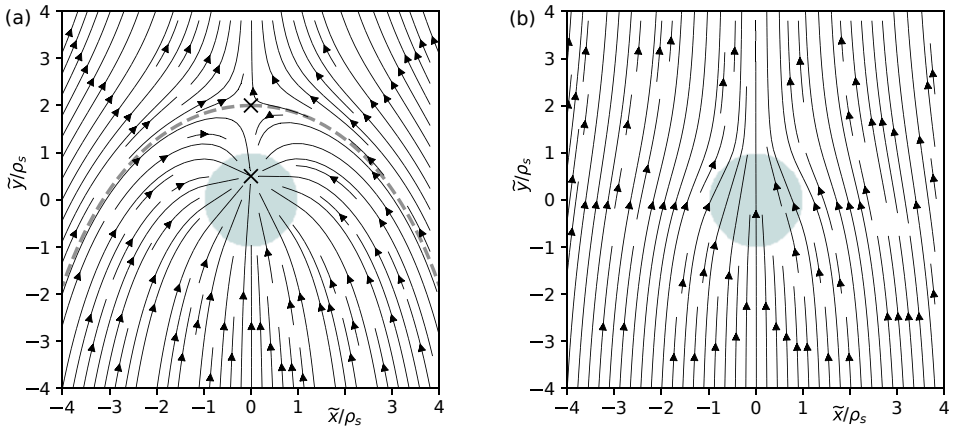

Figure 2: (a) Initial streamlines of $\mathbf{u}_l$ in the vicinity of a supercritical mass sink (grey disc) with $s_o/s_c = 2$. Each $\times$ marks the location of a stagnation point, whereas the thick dashed curve separates fluid drawn into the mass sink from untrapped fluid. (b) As in (a) but for $\mathbf{u}_l$ in the vicinity of a subcritical mass sink with $s_o/s_c = 0.5$. Note that the sink-centered polar coordinates defined in section 3.1 relate to the depicted Cartesian coordinates by $\rho = \sqrt{\tilde{x}^2 + \tilde{y}^2}$ and $\theta = \tan^{-1}(\tilde{y}/\tilde{x})$.

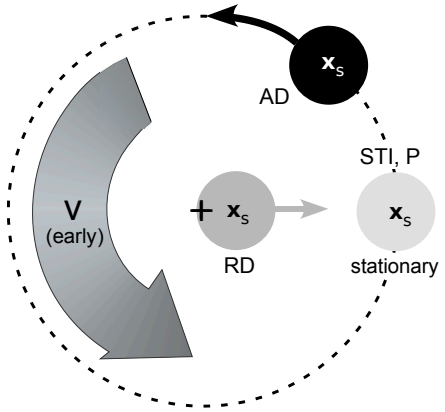

Figure 3: Illustration of possible positions and drifts of various sinks (shaded discs) within a shallow-water cyclone. The sink centers are labeled $\mathbf{x}_s$, whereas the domain center that coincides with $\mathbf{x}_{c0}$ is marked by the $+$. The arrows stemming from the AD and RD mass sinks show the directions of their drifts. The dashed circle centered on $\mathbf{x}_{c0}$ is the orbital path of the AD mass sink. The thick shaded arrow depicts the azimuthal velocity v of the cyclone prior to any substantial change of the vortex center. Note: although the figure shows multiple sinks, each simulation has only one.

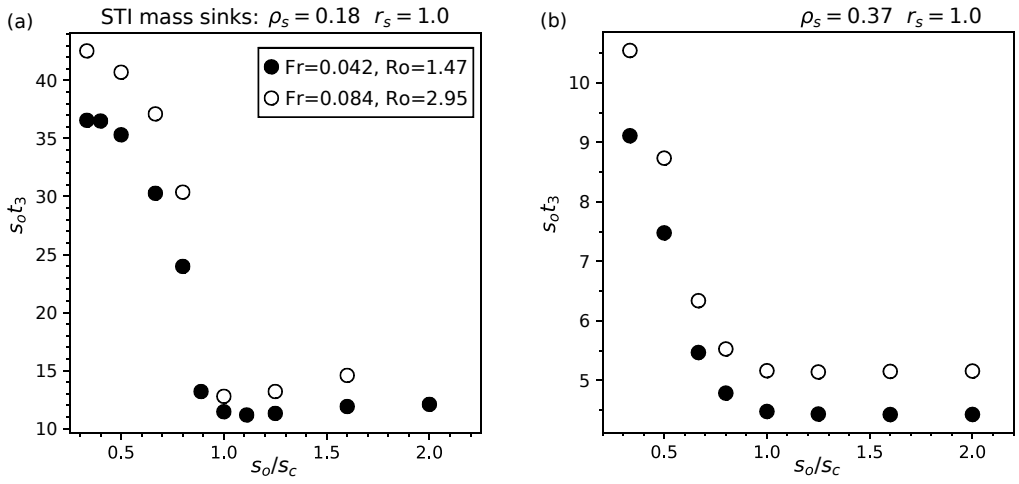

Figure 4: Normalized intensification period ($s_o t_3$) versus the ratio of the sink magnitude s_o over the theoretical critical value s_c for cyclones possessing STI mass sinks with $r_s = 1.0$ and (a) $\rho_s = 0.18$ or (b) $\rho_s = 0.37$. Filled and empty circles correspond to systems with distinct pairs of Fr and Ro, as indicated in the legend. Here and elsewhere [Figs. 5-7], the legend in (a) is for (b) as well.

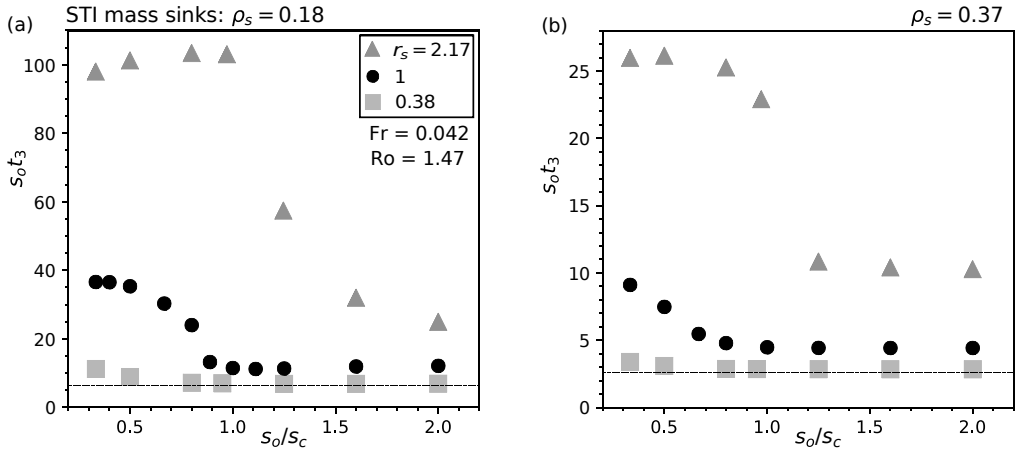

Figure 5: As in Fig. 4, but for cyclones possessing STI mass sinks at various radial distances from the initial vortex center. Different symbols represent systems with different values of r_s, as shown in the legend. The dashed lines show $s_o t_3$ when $r_s = 0$. In all cases, Fr=0.042 and Ro=1.47.

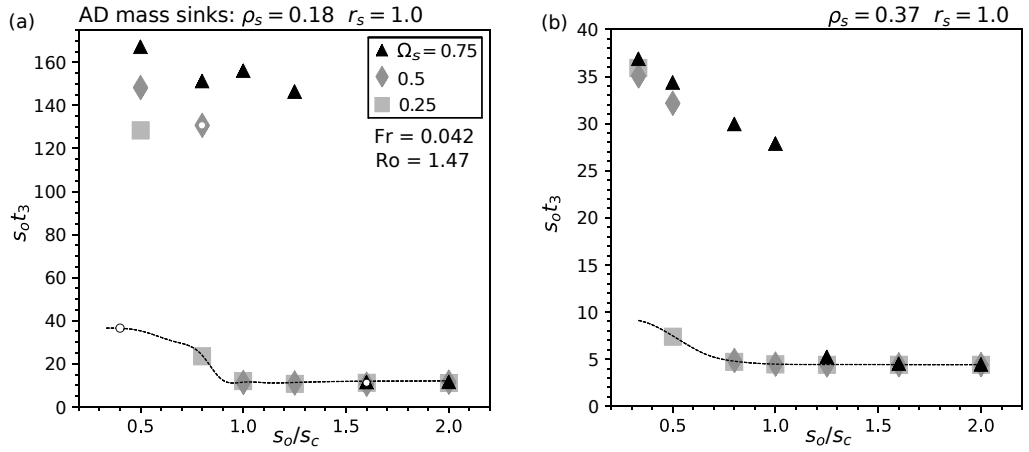

Figure 6: As in Fig. 4, but for cyclones possessing AD mass sinks with $r_s = 1$ and various angular velocities. Different shaded symbols represent systems with different values of Ω_s, as shown in the legend. The dashed curves show $s_o t_3$ when $\Omega_s = 0$. Small white circles in (a) mark the simulations mentioned near the end of section 4.2.2 with $s_o = 4.34$ and (left to right) $\Omega_s = 0$, 0.5 and 0.75. In all cases, Fr=0.042 and Ro=1.47.

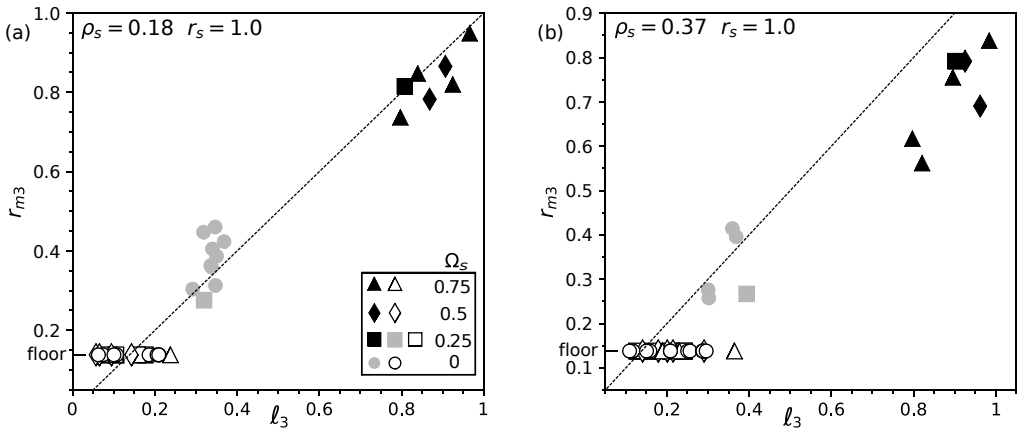

Figure 7: (a) Radius of maximal $\bar{v}$ in the vortex-centered reference frame (r_{m3}) versus the distance between the mass sink and vortex centers (ℓ_3) at the end of the intensification period for all systems possessing STI or AD mass sinks with $\rho_s = 0.18$ and $r_s = 1.0$. The shape of each symbol indicates the value of Ω_s. The shade of each symbol indicates the mode of intensification, as explained in the main text. The dashed line corresponds to $r_{m3} = \ell_3$. (b) As in (a) but for systems possessing mass sinks with $\rho_s = 0.37$.

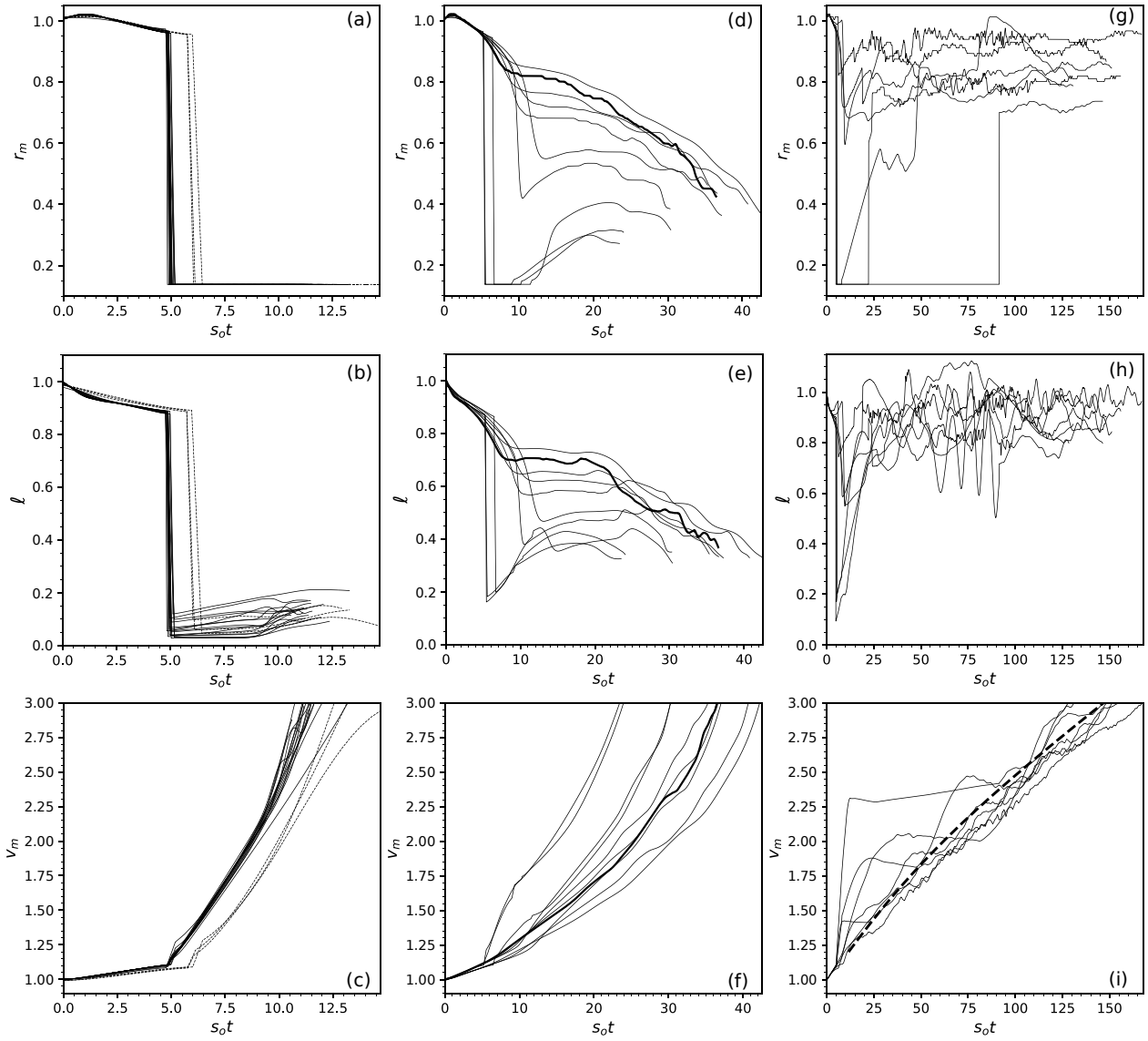

Figure 8: (a-c) Time series of (a) r_m, (b) ℓ and (c) v_m for all systems having supercritical STI or AD mass sinks with $\rho_s = 0.18$ and $r_s = 1$, represented by the white data in Fig. 7a. Solid (dashed) curves correspond to systems with Fr=0.042 (0.084) and Ro = 1.47 (2.95). (d-f) As in (a-c) but for systems with subcritical mass sinks represented by the grey data in Fig. 7a. All curves are solid regardless of differences in Fr and Ro. The thick solid curves correspond to the system analyzed in section 5, possessing an STI mass sink with $s_o/s_c = 0.33$. (g-i) As in (a-c) but for systems with subcritical AD mass sinks represented by the black data in Fig. 7a. The thick dashed curve in (i) corresponds to the maximum over r of $v_{\rm sym}(r,t)$ in the symmetrized system described in appendix C1.

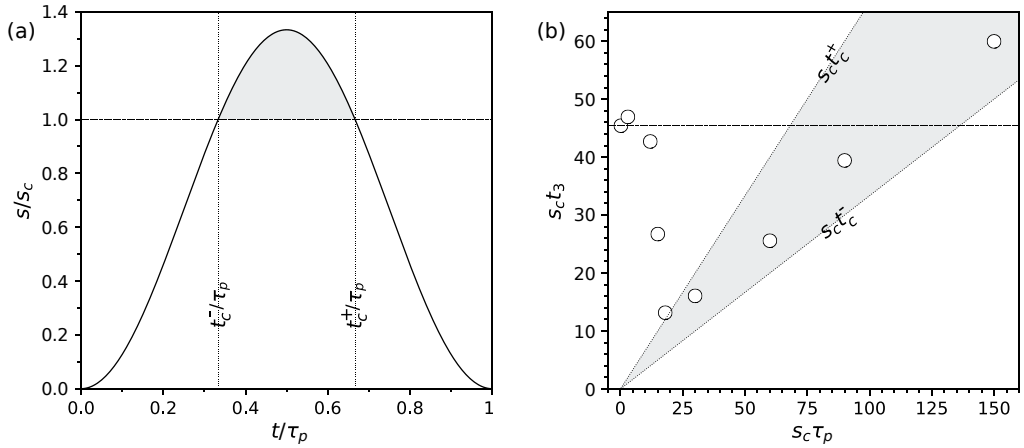

Figure 9: (a) Time dependence of the normalized magnitude s/s_c of a pulsating (P) mass sink with $s_p = 1.33s_c$ over the first wave cycle. (b) Wave period (τ_p) dependence of the intensification period (t_3, circles) of a cyclone possessing a P mass sink with $\rho_s = 0.18$, $r_s = 1$, and the waveform in (a). Both the wave period and intensification period are normalized to $1/s_c$. The Froude (Rossby) number is 0.042 (1.47). The shaded regions in (a) and (b) correspond to when s is supercritical during the first wave cycle. The horizontal dashed line in (b) shows $s_c t_3$ when the P mass sink is replaced with an STI mass sink having the same size and location with $s_o = s_p/2$.

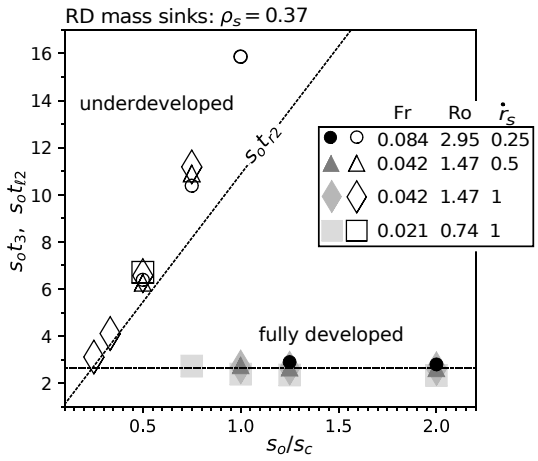

Figure 10: Graphical synopsis of the behavioral variation of cyclones possessing RD mass sinks with $\rho_s = 0.37$. As shown in the legend, different symbol-shapes correspond to systems with different settings for Fr, Ro and $\dot{r}_s$. *Shaded data*: normalized intensification period ($s_o t_3$ versus s_o/s_c) for cyclones that fully develop. *White data:* normalized time for separation ($s_o t_{\ell 2}$ versus s_o/s_c) between the mass sink and the center of a cyclone that fails to fully develop. The dashed lines are explained in the main text.

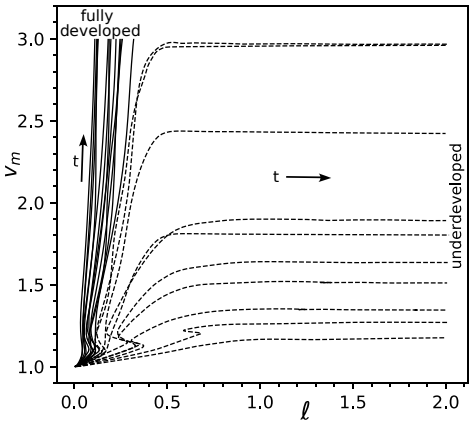

Figure 11: The ℓ-v_m phase space trajectories of cyclones that fully develop (solid curves) or fail to fully develop (dashed curves) when forced by RD mass sinks. The trajectories account for all systems in Fig. 10.

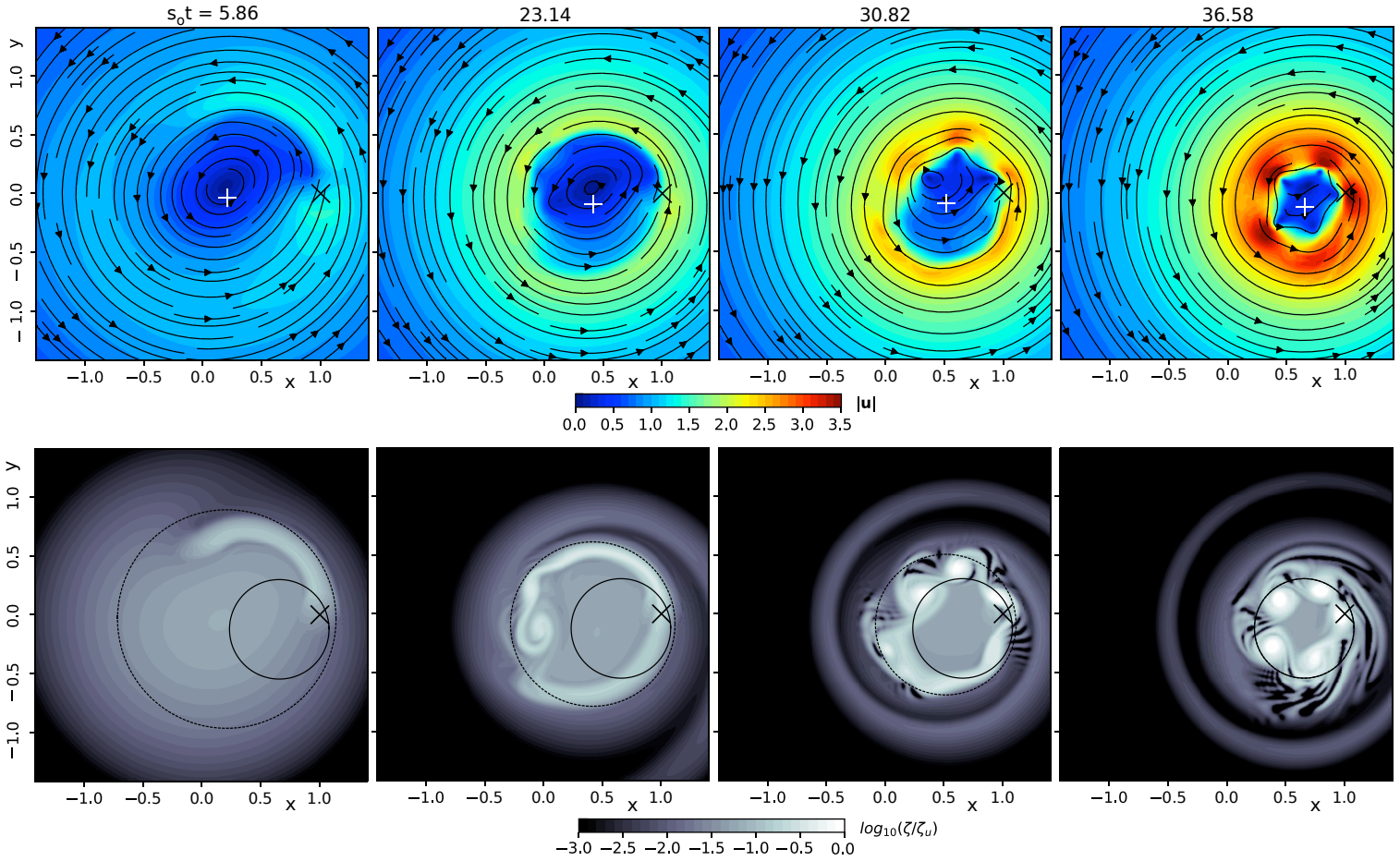

Figure 12: Development of a cyclone possessing an STI mass sink with $\rho_s = 0.18$, $r_s = 1$ and $s_o = 0.33 s_c$. The Froude and Rossby numbers are respectively 0.042 and 1.47. Top: snapshots of the streamlines and magnitude of the velocity field $\mathbf{u}$ in the stationary domain-centered reference frame. The white + marks the center of the vortex denoted in the main text by $\mathbf{x}_c$, whereas the black $\times$ marks the center of the mass sink denoted by $\mathbf{x}_s$. Bottom: corresponding snapshots of the logarithm of relative vorticity ζ divided by $\zeta_u = 54.3$. Regions with vorticity less than $10^{-3}\zeta_u$ (greater than ζ_u) are shaded black (white). The dashed circle is centered at $\mathbf{x}_c(t)$ and has a radius equal to $r_m(t)$. The solid circle is centered at $\mathbf{x}_c(t_3)$ and has a radius equal to $r_m(t_3)$, in which $t_3 = 36.58 s_o^{-1}$.

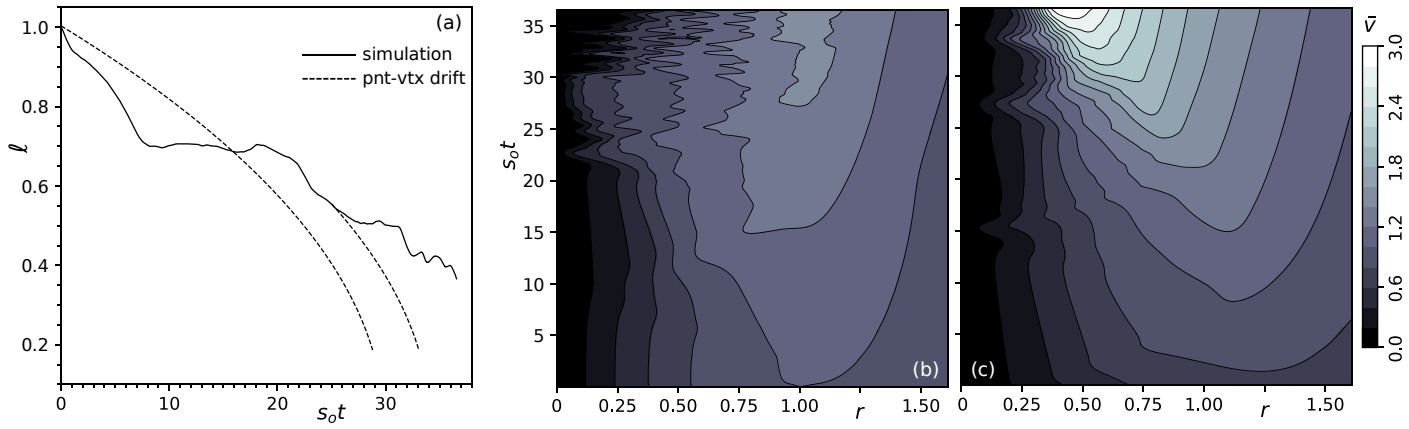

Figure 13: (a) Time series of ℓ for the simulation shown in Fig. 12. The simulation result (solid curve) is compared to hypothetical time series of ℓ (dashed curves) that would result upon replacing the relative vorticity distribution with a single point vortex at $\mathbf{x}_c$ and eliminating planetary vorticity at the beginning of the simulation or after moderate development has occurred. (b,c) Evolution of $\bar{v}$ in stationary coordinate systems centered at (b) $\mathbf{x}_{c0}$ and (c) $\mathbf{x}_c(t_3)$ for the same system; the contour interval is 0.2 units.

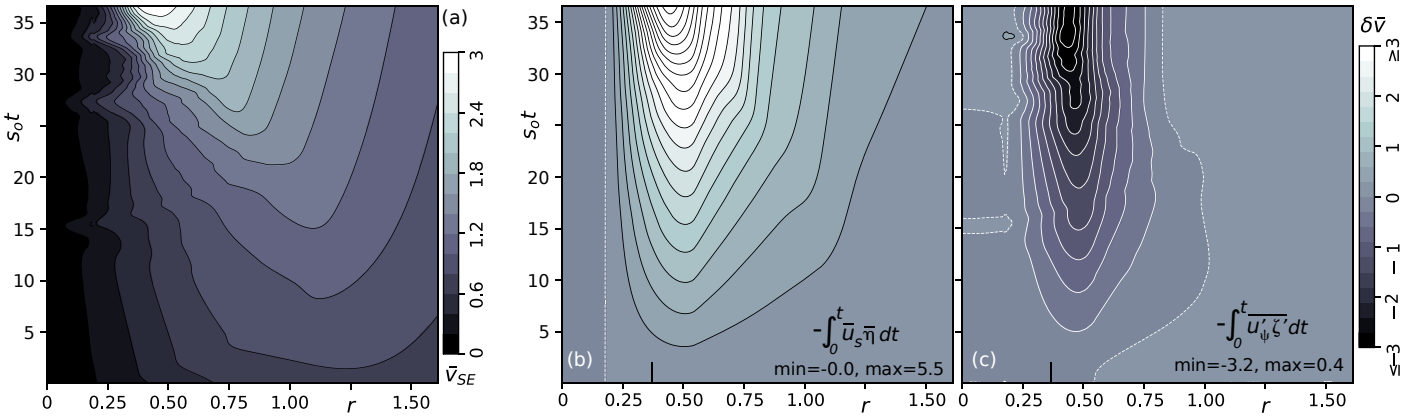

Figure 14: Analysis of the intensification of the cyclone in Fig. 12 in a stationary reference frame centered at $\mathbf{x}_c(t_3)$. (a) Precise reconstruction of $\bar{v}$ (denoted $\bar{v}_{SE}$) from a running time integral of the right-hand side of Eq. (19), in which $\bar{u}$ is obtained from a solution to the SE equation. The contour interval is 0.2 units. (b) Primarily positive contribution to the time integral from $-\bar{u}_s\bar{\eta}$. (c) Primarily negative contribution to the time integral from $-\overline{u'_\psi\zeta'}$. The grey scale to the right of (b) and (c) applies to the partial velocity change ($\delta\bar{v}$) in either panel. In (b) and (c), solid black/white contours correspond to positive/negative values of $\delta\bar{v}$ spaced 0.3 units apart; dotted white curves are zero contours; the tick extending upward from the bottom axis at $r = 0.37$ indicates where the center of the mass sink resides.

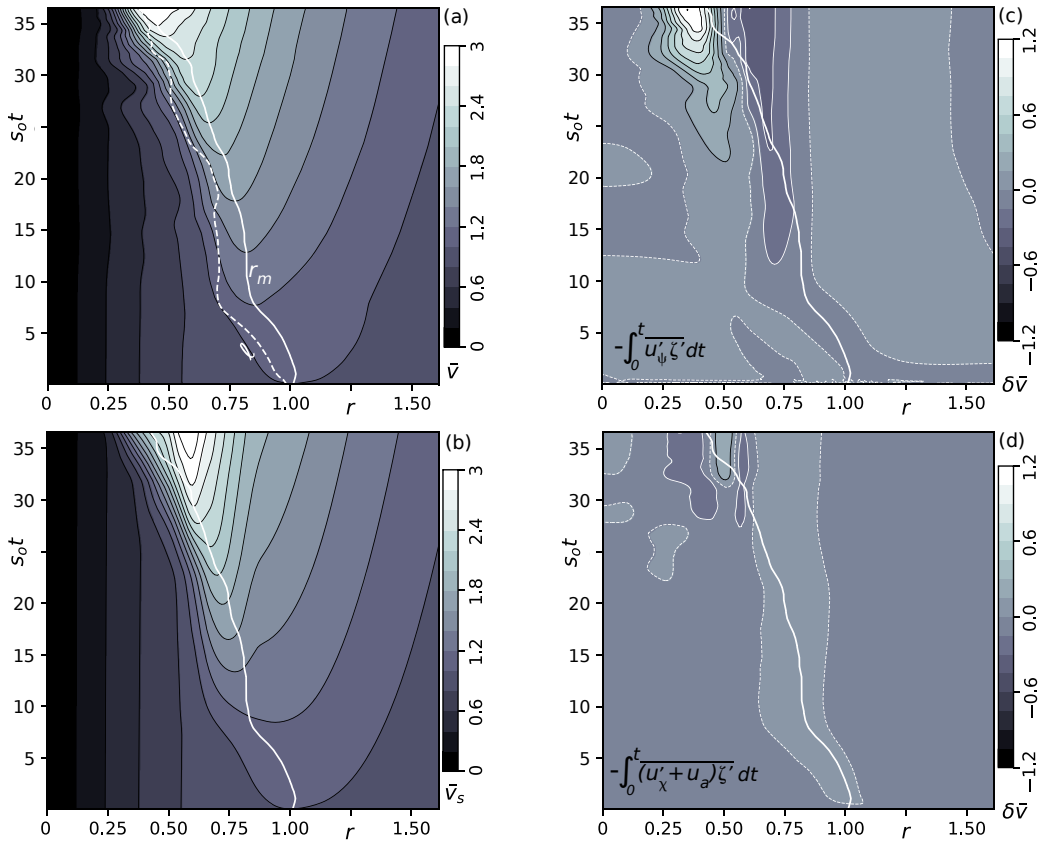

Figure 15: Intensification of the cyclone in Fig. 12 as seen in the moving vortex-centered reference frame. (a) Evolution of $\bar{v}$. Solid black contours are spaced 0.2 units apart. The thick solid white curve here and in (b)-(d) traces the radius of maximal $\bar{v}$. The thick dashed white curve traces the location of the sink center. (b) Hypothetical $\bar{v}$ (denoted $\bar{v}_s$) that would be generated by adding only the running time integral of $-\bar{u}_s\bar{\eta}$ to the initial conditions. The contour spacing is 0.2 units. (c,d) Running time integrals of (c) $-\overline{u'_\psi \zeta'}$ and (d) $-\overline{(u'_\chi + u_a)\zeta'}$. In (c) and (d), thin solid black/white contours correspond to positive/negative values; thin dotted white curves are zero contours; the contour interval is 0.15 units.

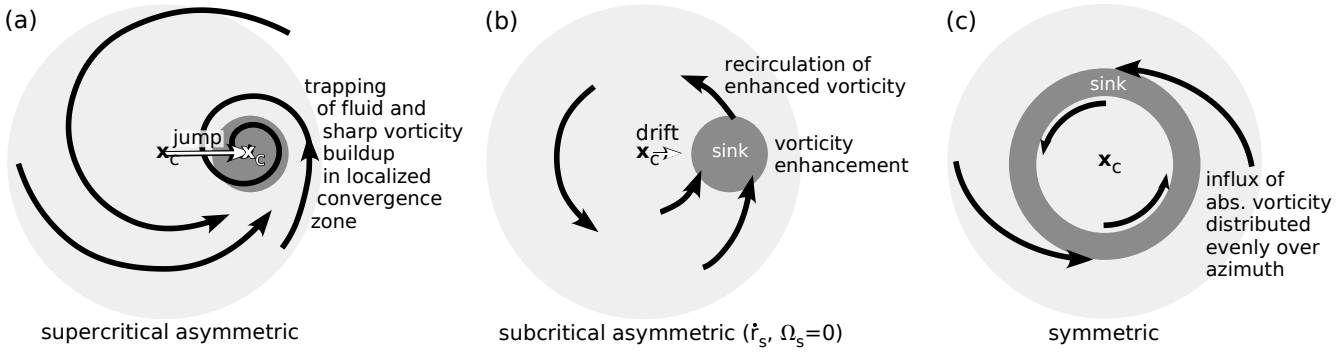

Figure 16: (a,b) Schematic illustrations of a shallow-water vortex undergoing (a) supercritical and (b) subcritical asymmetric intensification. Black curves with arrows convey the fluid motion within the vortex. Large light grey discs convey the presence of the broader vorticity distribution. The smaller mass sinks (convergence zones) shown in dark grey are taken to be stationary to simplify the illustrations. It is seen that the rotational center of the vortex ($\mathbf{x}_c$) abruptly jumps to the localized mass sink in the supercritical system, and more gradually drifts to the localized mass sink in the subcritical system. Other key aspects of the dynamics are noted in each panel. Bear in mind that if a subcritical mass sink has substantial azimuthal velocity, the displacement of $\mathbf{x}_c$ can be limited. (c) The symmetric intensification process reviewed in appendix C and depicted here for reference. In contrast to the asymmetric systems in (a) and (b), here the mass sink is annular and $\mathbf{x}_c$ remains fixed.

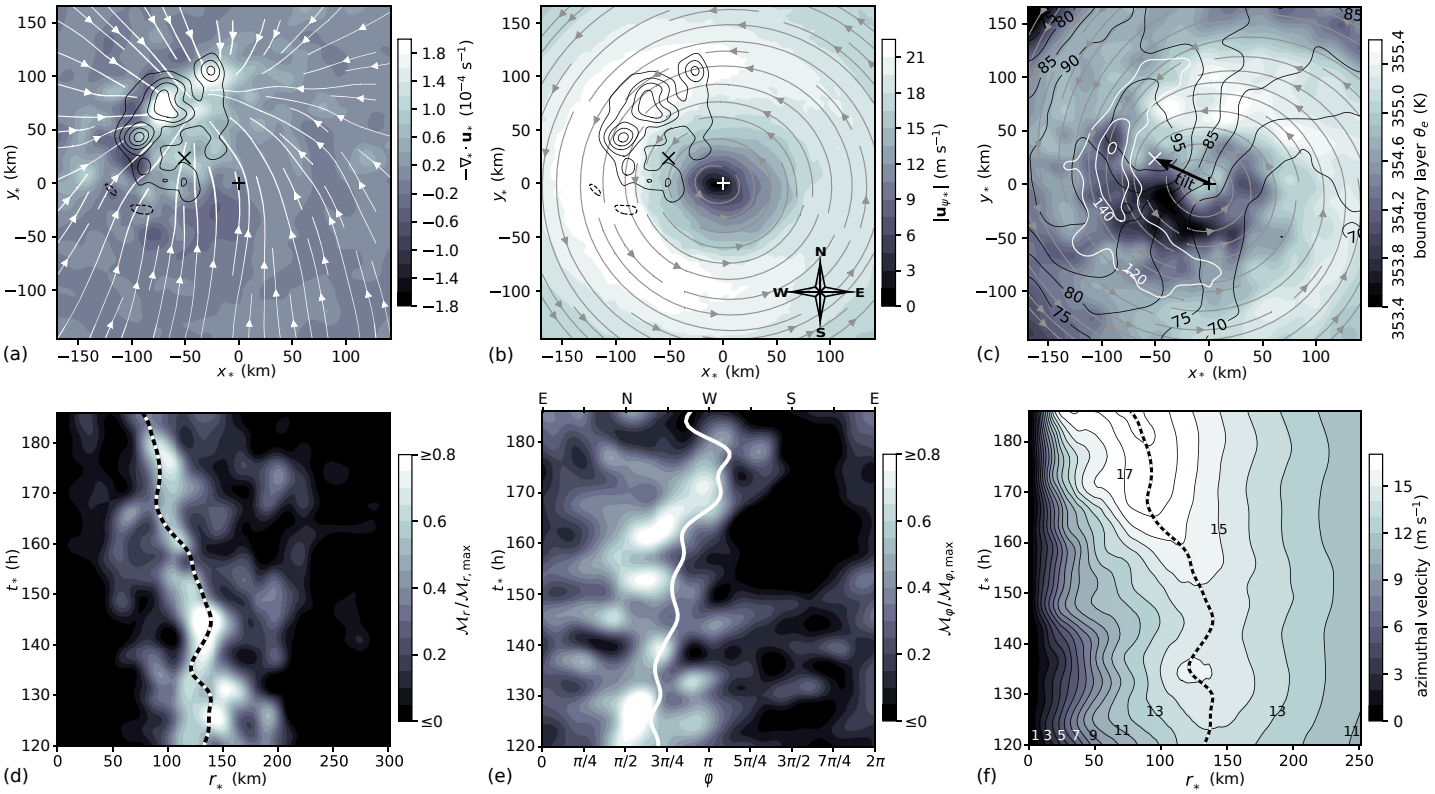

Figure A1: (a)-(c) Snapshot of the misaligned tropical cyclone in simulation DSPD-X400Z5 of SM20. All plotted fields are time-averaged between hours 160 and 166 of the simulation. The + marker shows the 6-h time-averaged center of rotation in the boundary layer, whereas the × marker shows the same at height $z_* \approx 7.7$ km. The former (latter) is denoted $\mathbf{x}_{cs}$ ($\mathbf{x}_{cm}$) in SM20. The downtilt direction points from + to ×. (a) Convergence of the lower tropospheric horizontal velocity field $\mathbf{u}_*$ (shading) and streamlines of the irrotational component $\mathbf{u}_{\chi*}$ of that velocity field (white curves). The black solid and dashed curves respectively represent positive and negative contours of vertical velocity w_* at $z_* = 8.9$ km. The contour spacing is 0.5 m s^{-1}, and the zero-line is excluded for clarity. (b) Magnitude (shading) and streamlines (grey curves) of the nondivergent component $\mathbf{u}_{\psi*}$ of the lower tropospheric velocity field. The black contours are as in (a). All lower tropospheric fields in (a) and (b) are vertically averaged between the sea-surface and $z_* = 3$ km. See section 5.2 for precise definitions of $\mathbf{u}_{\chi*}$ and $\mathbf{u}_{\psi*}$. (c) Boundary layer equivalent potential temperature (shading), boundary layer streamlines (grey curves), lower-middle tropospheric relative humidity (black contours; %), and the surface moist enthalpy flux where it is peaked (white contours; W m^{-2}). The boundary layer equivalent potential temperature and velocity field are vertically averaged over the interval $0 < z_* < 1$ km, whereas the lower-middle tropospheric relative humidity is averaged over the interval $2.3 < z_* < 7.7$ km. The convergence distribution in (a), w_* in (a) and (b), and all moist-thermodynamic fields in (c) are Gaussian smoothed in x_* and y_* with a standard deviation parameter of 6.25 km. (d)-(e) Hovmöller plots of the convergence profiles $\mathcal{M}_r$ and $\mathcal{M}_\varphi$ normalized to their maximum values over the depicted time frame. $\mathcal{M}_r$ ($\mathcal{M}_\varphi$) is Gaussian smoothed with standard deviation parameters of 6.25 km in r_* ($\pi/16$ radians in φ) and 2 h in t_*. (f) Hovmöller plot of the φ-averaged azimuthal velocity ($\bar{v}$) at $z_* = 25$ m with contour labels in m s^{-1}. The dashed curves in (d) and (f) trace the radius of maximal $\bar{v}$, whereas the white curve in (e) traces the orientation angle of the tilt vector depicted in (c).

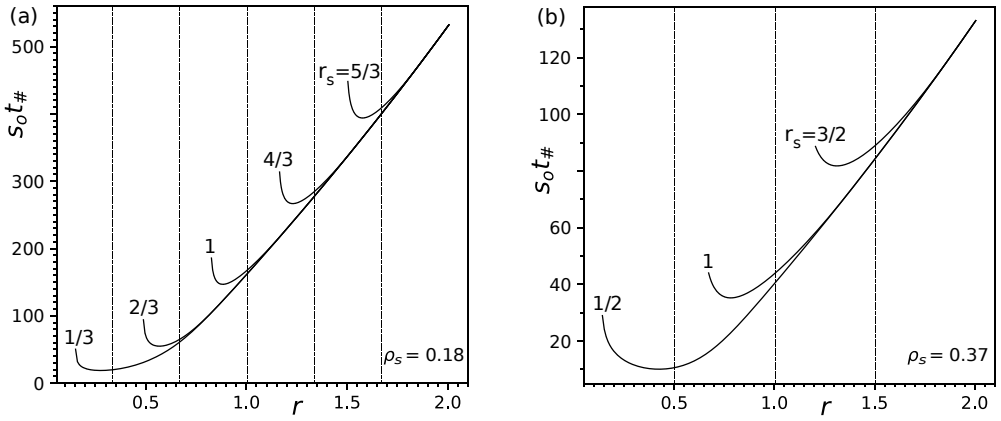

Figure C1: (a) Normalized time $s_o t_\#$ required to increase $v_{\rm sym}$ to 3 at a given radius r in a cyclone possessing an annular mass sink with $\rho_s = 0.18$ and an adjustable central radius (r_s). Different curves are for systems with different values of r_s, as indicated in the graph. The dashed vertical grid lines coincide with the locations of r_s. The Rossby number of each system is 1.47. (b) As in (a) but for cyclones possessing mass sinks with $\rho_s = 0.37$.